Modelling wintertime sea-spray aerosols under Arctic Haze conditions

Eleftherios Ioannidis[1,a], Kathy S. Law[1], Jean-Christophe Raut[1], Louis Marelle[1], Tatsuo Onishi[1], Rachel M. Kirpes[2], Lucia M. Upchurch[3,6], Thomas Tuch[4], Alfred Wiedensohler[4], Andreas Massling[5], Henrik Skov[5], Patricia K. Quinn[6], and Kerri A. Pratt[2,7]

[1]Sorbonne Université, UVSQ, CNRS, LATMOS, Paris, France
[2]Department of Chemistry, University of Michigan, Ann Arbor, Michigan, USA
[3]Cooperative Institute for Climate, Ocean, and Ecosystem Studies, University of Washington, Seattle, WA USA
[4]Leibniz Institute for Tropospheric Research, Leipzig, 04318, Germany
[5]Department of Environmental Science, iClimate, Aarhus University, Denmark
[6]Pacific Marine Environmental Laboratory, National Oceanic and Atmospheric Administration, Seattle, Washington 98115, United States
[7]Department of Earth and Environmental Sciences, University of Michigan, Ann Arbor, Michigan, USA
[a]now at: Department of Earth Sciences, Vrije Universiteit, Amsterdam, the Netherlands

Correspondence: Eleftherios Ioannidis (eleftherios.ioannidis@latmos.ipsl.fr, elefth.ioannidis@gmail.com) and Kathy S. Law (Kathy.Law@latmos.ipsl.fr)

Abstract. Anthropogenic and natural emissions contribute to enhanced concentrations of aerosols in the Arctic winter and early spring with most attention focusing on anthropogenic aerosols contributing to so-called Arctic Haze. Less well-studied wintertime sea-spray aerosols (SSA) under Arctic Haze conditions are the focus of this study since they can make an important contribution to wintertime Arctic aerosol abundances. Analysis of field campaign data also shows evidence for enhanced local

5 sources of SSA including marine organics at Utqiaġvik (formerly known as Barrow, in northern Alaska, United ~~Statmes~~States) during winter 2014. Models tend to underestimate sub-micron, and overestimate super-micron, SSA in the Arctic during winter, including the base version of the Weather Research Forecast, coupled with chemistry (WRF-Chem) model used here, which includes a widely used SSA source function based on *Gong et al. (1997)*. Quasi-hemispheric simulations for winter 2014 including updated wind-speed and sea-surface temperature (SST) SSA emission dependencies, and sources of marine ~~SSA~~

10 sea-salt organics and sea-salt-sulphate ~~leads~~ lead to significantly improved model performance compared to observations at remote Arctic sites, notably for coarse mode sodium and chloride which are reduced. The improved model also simulates more realistic contributions of SSA to inorganic aerosols at different sites, ranging from 20-93% in the observations. Two thirds of the improved model performance is from inclusion of the dependence on SSTs. Simulation of nitrate aerosols is also improved due to less heterogeneous uptake of nitric acid on SSA in the coarse mode and related increases in fine mode

15 nitrate. This highlights the importance of interactions between natural SSA aerosols and inorganic anthropogenic aerosols contributing to Arctic Haze. Simulation of organic aerosols and the fraction of sea-salt sulphate are also improved compared to observations. However, the model underestimates episodes with elevated observed concentrations of SSA components, and sub-micron non-sea-salt sulphate at some Arctic sites, notably at Utqiaġvik~~(sub-micron aerosols).~~. Possible reasons are explored in higher resolution runs over northern Alaska for periods corresponding to a Utqiaġvik field campaign in January and

February ~~2014,~~ 2014. The addition of a local source of ~~SSA~~ sea-salt marine organics, based on the campaign data, increases modelled organic aerosols over northern Alaska. However, ~~underestimation compared to~~ comparison with previous available data suggests that local natural sources from open leads as well as local anthropogenic sources are underestimated in the model. Missing local anthropogenic sources may also explain low modelled (sub-micron) non-sea-sulphate at Utqiaġvik~~(and certain other Arctic sites)~~. The introduction of a higher wind speed dependence for sub-micron SSA emissions, also based on Arctic data, reduces biases in modelled sub-micron SSA while sea-ice fractions, including open leads, are shown to be an important factor controlling modelled super-micron, rather than sub-micron, SSA over the north coast of Alaska. The regional results presented here show that ~~that~~ modelled SSA are more sensitive to wind speed dependence, but that realistic modelling of sea-ice distributions is needed for simulation of local SSA, including marine organics. This study supports findings from the Utqiaġvik field campaign that open leads are the primary source of fresh ~~,~~ and aged SSA, including marine organic aerosols, during wintertime at Utqiaġvik and do not suggest an influence from blowing snow and frost flowers. To improve model simulations of Arctic wintertime aerosols, new field data on processes influencing wintertime SSA production, in particular for fine mode aerosols, are needed as well as improved understanding about possible local anthropogenic sources.

1 Introduction

The Arctic region is warming faster than any other region on Earth due to carbon dioxide, in particular, and also due to short-lived climate forcers like methane, tropospheric ozone and aerosols *(AMAP, 2015; Allan, 2021)*. During winter and early spring, aerosols also affect clouds (aerosol-cloud indirect effects) and, more specifically, cloud droplet number ~~concentration~~ concentrations and size by increasing the long-wave emissivity of clouds (long-wave warming effect) *(Zhao and Garrett, 2015; Horowitz et al., 2020)*. At this time of year, elevated aerosol concentrations of black carbon (BC), nitrate (NO_3^-), non-sea salt (nss) sulphate (SO_4^{2-}) and organic aerosols (OA) are observed in the Arctic, a phenomenon known as Arctic Haze *(Rahn and McCaffrey, 1980; Barrie et al., 1994; Quinn et al., 2002)*, due to transport of anthropogenic aerosols and precursors from mid-latitude sources as well as within-Arctic emissions *(Heidam et al., 2004; Quinn et al., 2007; Law et al., 2014, 2017; Schmale et al., 2018)*. Natural aerosol sources such as dust, volcanic emissions and sea-spray aerosols (SSA) also contribute to wintertime Arctic aerosol burdens *(Barrie and Barrie, 1990; Quinn et al., 2002; Zwaaftink et al., 2016; Kirpes et al., 2018)*, with SSA also peaking in the wintertime *(Schmale et al., 2022)*. It is important to quantify wintertime natural aerosols, as well as anthropogenic components, since they can affect the Arctic radiative budget via indirect effects *(Schmale et al., 2018)*. There are also important interactions between SSA and anthropogenic components via heterogeneous uptake on SSA surfaces leading to inorganic aerosol formation *(Su et al., 2022)* which can influence the ability of models to simulate Arctic Haze. In this study, we focus on SSA under wintertime Arctic Haze conditions.

SSA are produced by bubble bursting (jet-drop and film-drop formation) on the sea surface due to wind stress during whitecap formation *(Monahan et al., 1986)*. SSA emissions also depend on sea surface temperatures (SSTs) and salinity *(Jaeglé et al., 2011; Sofiev et al., 2011; Revell et al., 2019)*. Frost flowers and blowing snow have also been proposed as a source in polar regions during wintertime *(Xu et al., 2013; Huang and Jaeglé, 2017)*. SSA is composed primarily of sodium

(Na^+), chloride (Cl^-), organics and sea-salt (ss) SO_4^{2-}. SSA may influence cloud formation, including Arctic mixed-phase clouds *(Adachi et al., 2022)*, since they can act as cloud condensation nuclei (CCN) *(Quinn et al., 2017)*, or organics may contribute to ice nucleating particles (INPs) *(Burrows et al., 2013)*. Arctic warming is leading to a decrease in summer sea-ice and thinner sea-ice during wintertime *(Stroeve et al., 2012)*. Increases in the area of the open ocean or more open leads in sea-ice may increase winter SSA over Arctic coastal regions, potentially influencing radiative forcing *(Ma et al., 2008; Eidhammer et al., 2010; Partanen et al., 2014; Schmale et al., 2022)*.

The ability of models to capture wintertime Arctic aerosols has largely focused on the evaluation of anthropogenic Arctic Haze components, in particular BC and SO_4^{2-} (e.g. *Eckhardt et al. (2015)*,*Whaley et al. (2022)*). *Whaley et al. (2022)* showed that, in general, models underestimate SO_4^{2-} and BC in winter. Very few model studies have assessed both anthropogenic and natural aerosols, like SSA, and these models do not generally make the distinction between nss and ss components of SO_4^{2-} or OA. A recent study by *Moschos et al. (2022a)* estimated that wintertime Arctic OA have largely anthropogenic origins but a possible contribution from local marine organics was not considered. An analysis of single-particle data from a field campaign near Utqiaġvik, northern Alaska, in winter 2014, showed that, in addition to organic-sulphate Haze aerosols, there were abundant fresh SSA, based on the presence of Na^+, Cl^-, magnesium and sulphur in ratios similar to seawater, that were produced locally from open leads and included marine OA originating from secretions from sea ice algae and bacteria *(Kirpes et al., 2018, 2019)*. It can be noted that during winter, fresh SSA can be a significant fraction of particulate matter, contributing up to 40% of super-micron (1 to 10 μm particle diameter) and 25% of sub-micron (up to 1 μm particle diameter) aerosol mass *(Quinn et al., 2002)*. *Kirpes et al. (2018)* also observed aged SSA, which made up the majority of the sub-micron number fraction during their campaign at Utqiaġvik. These aged SSA were internally mixed with secondary SO_4^{2-}, or both SO_4^{2-} and NO_3^-, and Cl^- was depleted, indicating that multi-phase reactions had occurred during transport. The aged SSA were sampled in air masses influenced by background Arctic Haze and regional northern Alaskan oil field emissions. Their findings support an earlier analysis of Ny-Alesund (Svalbard) data showing that aged SSA were always internally mixed with NO_3^-, SO_4^{2-}, and organics *(Chi et al., 2015)*. In fact, heterogeneous reactions occurring on the surface of SSA, involving uptake of sulphuric, nitric or organic acids, and associated Cl^- displacement, are more evident in aged SSA *(Chi et al., 2015)*. *Chen et al. (2016)* showed that uncertainties in modelled SSA can have a significant impact on sub-micron and super-micron NO_3^- due to heterogeneous uptake of nitric acid (HNO_3) on SSA which produces NO_3^-. Uptake of sulphuric acid on SSA in the marine boundary layer can result in SO_4^{2-} production *(Alexander et al., 2005)*. *Li et al. (2018)* and *Wu et al. (2019)* emphasised the importance of heterogeneous reactions occurring on SSA for improved simulation of SO_4^{2-} and NO_3^- size distributions. Since nitric and sulphuric acid have largely anthropogenic origins this highlights important links between natural SSA and anthropogenic inorganic aerosols.

This study is motivated by the findings of *Kirpes et al. (2018, 2019)* on wintertime Arctic aerosols, including SSA coated with marine organics, in northern coastal Alaska. Our main objectives are to assess the ability of the regional atmospheric Weather Research Forecast, coupled with chemistry, (WRF-Chem) model to simulate wintertime aerosols, in particular SSA, under Arctic Haze conditions, and to examine model sensitivity

to processes which may be influencing SSA aerosols over northern Alaska, in particular. We also assess the observed and modelled contribution of SSA to total inorganic aerosols during Arctic wintertime.

Firstly, we focus on improving the model SSA emission scheme over the wider Arctic during winter. This includes updating the wind speed dependence, including a dependence on SSTs, and adding sources of marine OA and ss-SO_4^{2-}. Due to the links between SSA and other inorganic aerosols, contributing to Arctic Haze, model results are evaluated against observations of all aerosol components at remote Arctic sites. To our knowledge, these aspects have not been considered in previous studies using either WRF-Chem or other models (e.g. *Whaley et al. (2022)*). Secondly, we investigate the sensitivity of modelled SSA to processes influencing SSA, including organics and other inorganic aerosols, at Utqiaġvik using the improved model run at higher resolution over northern Alaska for periods corresponding to the *Kirpes et al. (2018, 2019)* campaign. The sensitivity of the model results to the addition of a local source of marine organics, wind speed dependence and sea-ice fractions are investigated based on the findings of this field campaign and other data collected in the Arctic. A possible contribution from frost flowers or blowing snow is also considered.

The model setup, including anthropogenic and natural emissions, is described in Section 2. The aerosol observations used to evaluate the model are introduced in Section 3. Details about the SSA emission scheme in the base model version, together with improvements to this scheme, are presented in Section 4. Evaluation of simulated SSA, as well as other inorganic and organic aerosols, against Arctic observations, are presented in Section 5, together with an estimation of the contribution of SSA to total inorganic aerosols. Results from the regional study over northern Alaska are presented in Section 6. The implications of our findings for the simulation of SSA under wintertime Arctic Haze conditions are presented in Section 7 (Conclusions).

2 WRF-Chem

2.1 Model Setup

WRF-Chem model version 3.9.1.1 is used in this study. It is a fully coupled, online meteorological and chemical transport mesoscale model *(Grell et al., 2005; Fast et al., 2006)*. Recent improvements to the WRF-Chem model over the Arctic are included in the version used here *(Marelle et al., 2017)*. The model setup, including meteorological and chemical schemes, is shown in Table 1. Briefly, Yonsei University (YSU - boundary layer), Model Version 5 similarity (MM5 - surface layer) and ~~Noah-Multiparameterization~~ NOAH-Multiparameterization Land Surface Model (NOAH MP, land surface model) are used. More details about the NOAH MP scheme are given in APPENDIX A.

The well-known processes for aerosols in the atmosphere, like nucleation, evaporation, coagulation, condensation, dry deposition, aerosol/cloud interactions and aqueous chemistry, are included in the Model for Simulating Aerosol Interactions and Chemistry (MOSAIC, *Zaveri et al. (2008)*) aerosol scheme used here. MOSAIC treats all the major aerosol species, such as SO_4^{2-}, NO_3^-, Cl^-, ammonium (NH_4^+), Na^+, calcium (Ca^{2+}), BC, and OA. Reactive inorganic species such as potassium (K^+) and magnesium (Mg^{2+}) are not modelled in MOSAIC. The size distribution of each aerosol species is represented by eight bins, from 0.0391 micrometres (μm) to 10 μm: [0.0391 to 0.0781], [0.0781 to 0.1562], [0.1562 to 0.3125], [0.3125 to 0.625], [0.625 to 1.25], [1.25 to 2.5], [2.5 to 5.0] and [5.0 to 10.0] in μm. Each bin is assumed to be internally mixed, and both mass

Table 1. WRF-Chem model setup. The source functions for sea-spray emissions and their main updates are summarised below. CONTROL includes only *Gong et al. (1997)*, while HEM_NEW includes updates to the SSA emission scheme. See text for details.

Parameterisation scheme	Options
Physics (WRF)	
Planetary boundary layer	Yonsei University (YSU) - *(Hong et al., 2006)*
Surface layer	Pennsylvania State / NCAR Mesoscale
	Model Version 5 (MM5) similarity
	(Grell et al., 1994; Jiménez et al., 2012)
Land surface	NOAH MP *(Niu et al., 2011)*
Microphysics	Morrison *(Morrison, 2009)*
Shortwave & Longwave radiation	Rapid Radiative Transfer Model (RRTMG - *Iacono and D. (2008)*)
Cumulus parameterization	Kain-Fritsch with cumulus potential (KF-CuP)
	(Berg et al., 2013)
Chemistry (WRF-Chem)	
Aerosols	MOSAIC 8-bins *(Zaveri et al., 2008)*
Gas-phase chemistry	Statewide Air Pollution Research Center ~~SAPRC-99~~ (SAPRC)-99
	Modified dimethyl sulphide chemistry
	(Carter, 2000; Marelle et al., 2017)
Photolysis	Fast-J *(Wild et al., 2000)*
CONTROL	
Sea-salt emissions	*Gong et al. (1997)*
HEM_NEW (updates to *Gong et al. (1997)*)	
Sea-spray emissions (marine organics)	*Fuentes et al. (2010, 2011)*
Satellite wind speed dependence, SST dependence	~~*(Salisbury et al., 2014; Jaeglé et al., 2011)*~~ *Salisbury et al. (2014), Jaeglé et al. (2011)*
ss-SO_4^{2-} source	~~*(Kelly et al., 2010)*~~ *Kelly et al. (2010)*

and number are simulated. As a result, aerosols are aged when emitted (coagulated with other species). The MOSAIC version used in this study also includes 18 irreversible heterogeneous reactions (see Table 1 in *Zaveri et al. (2008)*), such as the reaction of HNO_3 on sodium chloride ($NaCl$) to form sodium nitrate ($NaNO_3$), with depletion of Cl^-. The reaction between $NaCl$ and ~~sulfuric~~ sulphuric acid (H_2SO_4) to produce sodium ~~sulfate~~ sulphate (Na_2SO_4), with associated Cl^- depletion, is also included. Nighttime chemistry, notably heterogeneous hydrolysis of dinitrogen pentoxide leading to HNO_3 formation, is also included *(Archer-Nicholls et al., 2014)*. The applied MOSAIC version includes secondary organic aerosol (SOA) formation from the oxidation of anthropogenic and biogenic species *(Shrivastava et al., 2011; Marelle et al., 2017)* and is combined with SAPRC-99 gas-phase chemistry. In the base model, OA is the sum of SOA and anthropogenic emissions of organic matter (OM). Aqueous chemistry in grid-scale *(Morrison, 2009)* and subgrid-scale clouds *(Berg et al., 2015)* is also included. Aerosol sedimentation in MOSAIC is calculated throughout the atmospheric column based on the Stokes velocity scheme, as described in *Marelle*

130 *et al. (2017)*. Wet removal of aerosols by grid-resolved stratiform clouds (precipitation) includes in-cloud and below-cloud removal by rain, snow, and graupel by Brownian diffusion, interception, and impaction mechanisms following *Easter et al. (2004)* and *Chapman et al. (2009)*. Wet-removal due to subgrid-scale convective clouds *(Berg et al., 2015)* is also included in this MOSAIC version and described in previous studies *(Marelle et al., 2017; Raut et al., 2017)*.
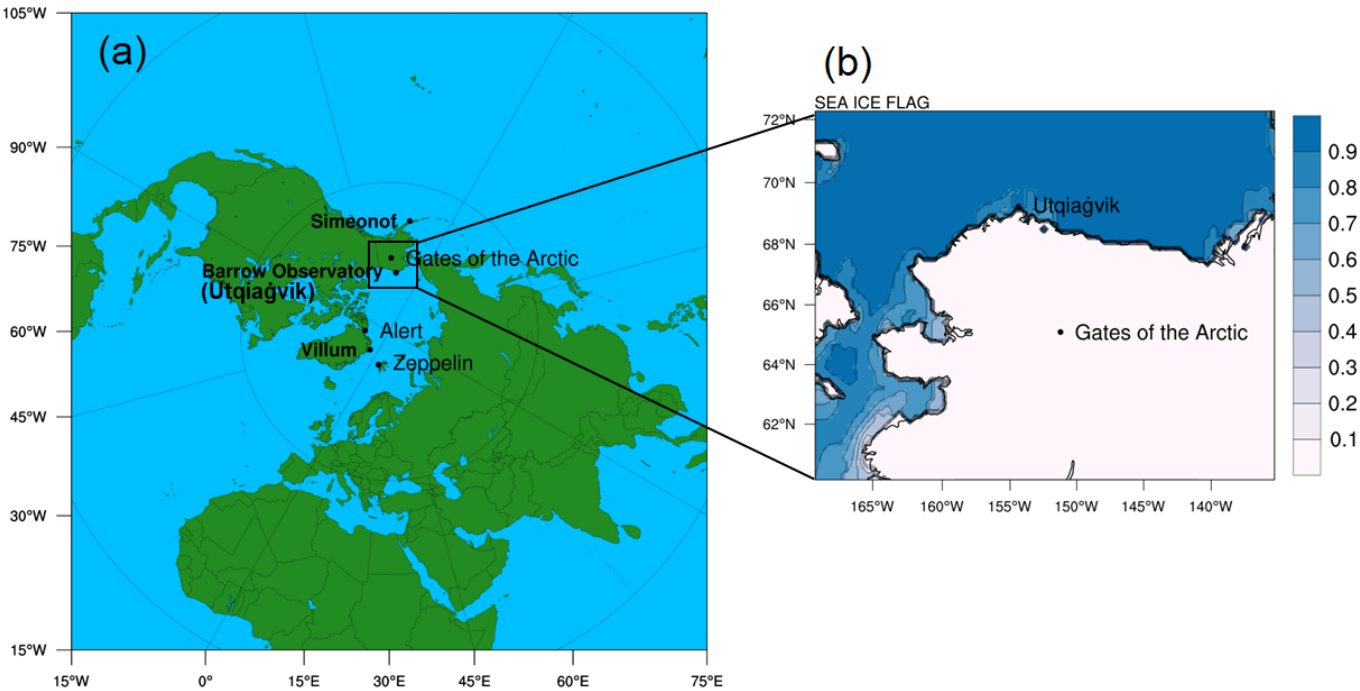
Figure 1. WRF-Chem simulation domains: (a) d01 is the 100km domain and (b) d02 is the 20km domain. d02 shows sea-ice fractions interpolated at 20km obtained from NCEP FNL ~~(at 1°x1° resolution *(NCEP, 2000)*)~~. See text for details.

2.2 Anthropogenic and natural emissions

135 Anthropogenic emissions are from the Evaluating the Climate and Air Quality Impacts of Short-Lived Pollutants version 6 (ECLIPSE v6b) inventory, with a resolution of 0.5° x 0.5° *(Whaley et al., 2022)*~~, including emissions of organic matter (OM)~~. Emissions of dimethyl-sulphide (DMS) and lightning nitrogen oxides (NO_x) are calculated online in the model (see *Marelle et al. (2017)* and references therein). Dust emissions in MOSAIC are calculated following *Shaw et al. (2008)*. Biogenic emissions for 2014 are calculated online using Model of Emissions of Gases and Aerosol from Nature (MEGAN) model

140 *(Guenther et al., 2012)*. Details about the treatment of SSA emissions and their improvement in the model are provided in Section 4 and summarised in Table 1.

2.3 Simulations

Two simulation domains on a polar stereo-graphic projection are used in this study, as shown in Figure 1. The first (parent) domain (d01) covers a large part of the Northern Hemisphere with 100 × 100km horizontal resolution. The boundary and initial conditions are derived from National Centres for Environmental Prediction Final meteorological reanalysis data (NCEP FNL) ~~meteorological reanalyses~~ and Model for OZone And Related chemical Tracers (MOZART, *Emmons et al. (2010)*) for atmospheric trace gases and aerosols. The nested domain (d02), run at a horizontal resolution of 20 × 20km, covers continental Alaska, a small area of northwest Canada, and the Chukchi and Beaufort Seas (see Fig. 1). 50 vertical levels and grid nudging are used for the 100km resolution domain, while spectral nudging, following *Hodnebrog et al. (2019)*, is implemented in the nested domain. WRF-Chem temperatures and winds are nudged at each dynamical step to the reanalysis, and updated every 6 hours, above the atmospheric boundary layer.

Two simulations at 100km are performed, one using the base model version (CONTROL) and one using CONTROL plus improvements to the SSA emissions (HEM_NEW) (see Section 4). They are run for 4 months from November 2013 until the end of February 2014, with the first two months considered as spin-up. The results are evaluated over the wider Arctic in Section 5. Results from HEM_NEW are then used as boundary conditions for regional runs over northern Alaska at 20 km for two different periods (23–28 January 2014 and 24–28 February 2014) corresponding to the Utqiaġvik campaign described earlier ~~(~~(*Kirpes et al., 2018, 2019*), KRP18 and KRP19 from now on ~~,~~(see also sub-section 3.2). In this case, the model is run for 4 days prior to the beginning of each campaign and considered as spin-up. Results from a series of sensitivity runs to examine processes affecting SSA on a regional scale are discussed in Section 6. In all runs, model results are output every 3h.

3 Aerosol Observations

The sites discussed in this section are shown in Figure 1.

3.1 Routine monitoring sites

Surface mass concentration data (for aerodynamic diameters (defined as d_a) < 10 μm), from ~~the~~ EMEP (European Monitoring and Evaluation Programme)~~dataBASe (EBAS-)~~, available via EBAS, for Zeppelin, Ny-Ålesund, Norway (78.9N, 11.88W) and Alert, Canada (82.5N, -63.3W), are used to evaluate the 100km model simulations together with total suspended particulate (TSP) (cutoff at 20 μm) data from Villum Research Station, Station Nord, Greenland (81.6N, -16.7W), referred to as Villum from now on. The data are collected on a daily (Zeppelin) and weekly (Villum, Alert) basis. At Alert, observations for Na^+, Cl^-, NO_3^- and total SO_4^{2-} measured with ion chromatography are used *(Sharma et al., 2019)*. This is also the case at Zeppelin *(Aas et al., 2021)*. At Villum, the same observations are collected using a filter-pack over a week and analysed using ion-chromatography (Cl^-, total SO_4^{2-}), and cation ~~ion chromatography~~ ion-chromatography (Na^+). For all the EBAS stations, observed inorganic aerosols (total SO_4^{2-}, NO_3^-) are converted to mass concentrations (μgm^{-3}), to compare to model results, using the ratio of molar weights of NO_3^-, SO_4^{2-} to molar weights of nitrogen or sulphur, respectively. With regard to measure-

ment uncertainties, EBAS documentation notes uncertainties ranging between 33% and 36% for Na^+, total SO_4^{2-}, NO_3^- and Cl^- at Alert. These high uncertainties may be related to uncertainties in the size cut-off of sub-micron filters. Uncertainties in coarse particle observations $(d_a < 10~\mu m)$ are based on the difference between high-volume (TSP) filters collected outside and sub-micron filters collected inside.

Fine mode $(d_a \leq 2.5~\mu m)$ mass concentration data from the Interagency Monitoring for Protected Visual Environments (IMPROVE) database is also used for model evaluation for Simeonof (55.3N, -160.5W), a sub-Arctic site on the ~~Aleutians islands~~Aleutian Islands, south of Alaska and an inland site, Gates of the Arctic (66.9N, -151.5W), GoA from now on, which is located 391 km south-east of Utqiaġvik town in northern Alaska (see Fig. 1). The samples are collected on-site over 24 hours every three days ~~, Malm et al. (1994)~~(Malm et al., 1994)). At these two sites observations of Na^+, Cl^-, organic carbon (OC), NO_3^- and total SO_4^{2-} are used. To compare with the OC observations at the two Alaskan sites, modelled OA is divided by 1.8, the reported ratio of ~~OM~~organic mass (OM)/OC in the documentation for these two stations *(Malm et al., 1994)*. ~~In this study, mass concentration data with d ≤ 2.5 μm are defined as fine mode aerosols, while d_a < 10 μm are defined as coarse mode aerosols.~~

Sub-micron $(d_a < 1.0~\mu m)$ and super-micron $(1.0 < d_a < 10~\mu m)$ surface mass concentration data from the National Oceanic and Atmospheric Administration (NOAA) Barrow Observatory (71.3N, -156.8W), near Utqiaġvik town (Utqiaġvik from now on), ~~is~~ are also used in this study, with daily and weekly temporal coverage, respectively. The sampling site is located 8 km northeast of Utqiaġvik town, 3km southwest of the Arctic Ocean, covered with snow during winter and 20m above mean sea level (msl), with a prevailing, east-northeast wind off the Beaufort Sea. Na^+, Cl^-, NO_3^- and total SO_4^{2-} mass concentrations are determined by ion chromatography *(Quinn et al., 1998)* and are sampled only for wind directions between 0 and 130 degrees (with 0 degrees indicating north). According to *Quinn et al. (2002)*, measurement uncertainties in sub-micron SSA components and nss-SO_4^{2-} are below $1.0 \pm 6.1\%~\mu gm^{-3}$ (concentration $\pm$ 95% uncertainty). The uncertainties in sub-micron NH_4^+ are below $0.2 \pm 7.8\%~\mu gm^{-3}$. The uncertainties in super-micron aerosols can be up to 7 times higher than for sub-micron aerosols, since 7 daily sub-micron samples are collected for every (weekly) super-micron sample. Measurement uncertainties are also due to sampling losses in the inlets. At Utqiaġvik, for particles with a diameter up to 10 μm, losses in the inlet system, from all loss mechanisms, are estimated to be less than 10%, and losses of particles between the diameters of 0.01 and 1 μm are below 5% *(Sheridan et al., 2001)*.

At each site observed ss-SO_4^{2-} is calculated from observed Na^+ concentrations and the mass ratio of SO_4^{2-} to Na^+ in seawater of 0.252 *(Bowen et al., 1979; Calhoun et al., 1991)* and nss-SO_4^{2-} is the difference between total SO_4^{2-} and ss-SO_4^{2-}. Note that, in some cases, observed nss-SO_4^{2-} has small negative concentrations, due to depletion of ss-SO_4^{2-} through fractionation processes *(Quinn et al., 2002)*. We note that, apart from the sub-micron observations at Utqiaġvik and fine mode observations from the IMPROVE database, there are no other sub-micron or fine-mode observations collected routinely in the Arctic, as also reported recently by *Schmale et al. (2022)*. Finally, data from a scanning mobility particle sizer (SMPS), located at Utqiaġvik, are used~~and measures the particle size distribution~~, providing measurements of particle number distributions at high temporal resolution, with a size range from 8.6 to 985 nm (0.0086 to 0.985 μm). No wind speed criteria have been applied to exclude local (Utqiaġvik town) or regional (e.g. North Slope of Alaska oil fields) pollution. Here, only SMPS observations at Utqiaġvik

are used since observations at the other Arctic sites used in this study are not available for winter 2014, as discussed by *Freud et al. (2017)*.

210   The model Stokes aerosol diameter is converted to d_a using the *Seinfeld and Pandis (1998)* formula. Thus, the diameter of modelled sub-micron particles is up to 0.73 μm (including the first four MOSAIC bins and a fraction of the 5th bin), and super-micron particle diameters are between 0.73 to 7.3 μm (fraction 5th bin, 6th and 7th bins and fraction 8th bin). Seven MOSAIC bins and a fraction of the 8th bin are used (modelled Stokes $r_d \leq 7.3$ μm) to compare with Alert and Zeppelin observations ($d_a < 10$ μm). All model aerosol bins are used to compare with observations at Villum, where the observations are reported as

215   TSP. For each site, modelled aerosols are estimated at the same conditions (temperature, pressure) as the reported observations. Also, observed total OC is assumed to include SOA, anthropogenic OA emissions and marine organics. Thus, from now on it will be referred to as tOC, to distinguish from OA defined earlier and OM. Aerosol measurements with different size ranges (up to 1.0 μm, 2.5 μm, and 10 μm) are used to validate the model results.

3.2   Campaign data

220   Details about the field campaign (January 23–27 and February 24–28, 2014) measurements near Utqiaġvik, Alaska can be found in KRP18 and KRP19. Briefly, atmospheric particles were collected using a rotating micro-orifice uniform deposition impactor located 2m above the snow surface at a site located 5km across the tundra from the NOAA Barrow Observatory and inland from the Arctic Ocean. The sampled particles were analysed by computer-controlled scanning electron microscopy with energy scattering X-ray spectroscopy (CCSEM-EDX) to determine the individual particle morphology and elemental

225   composition. The analysed samples were collected either during daytime or nighttime, and only when wind directions were between 75 and 225 degrees, to minimise local pollution influence. Data analysis provided information about the different chemical components as a fraction of the total number of particles sampled observed during the campaign.

4   Model SSA emission treatments and updates

This section introduces the treatment of SSA emissions in the base model version of WRF-Chem using the MOSAIC aerosol

230   scheme, followed by a description of the updates to the SSA emissions implemented in the model. The model is run with the original scheme (CONTROL run) and with the updates (HEM_NEW run). Results from both runs are evaluated against observations in the Arctic, in Section 5.

4.1   SSA emissions - CONTROL run

SSA ~~emissions~~ emission fluxes (F) in MOSAIC are calculated per particle radius r, with 1000 sub-bins per MOSAIC bin,

235   assuming that sea-salt is a simple mix of pure NaCl and using the density function dF/dr (in particles $m^{-2}s^{-1}\mu m^{-1}$) based on *Gong et al. (1997)* (G97 from now on). The G97 source function represents the rate that seawater droplets form per unit area (sea surface) and per increase of particle radius. The fraction of Na^+ is calculated using the molar weight of Na^+ and Cl^- and then the fraction of Cl^- is estimated, with the total being equal to 1. The G97 density function derived from the source function

is based on laboratory experiments described in *Monahan et al. (1986)* (MO86 from now on):

$$\frac{dF}{dr} = 1.373 \times U_{10}^{3.41} \times r^{-3}(1 + 0.057 \times r^{1.05}) \times 10^{1.19e^{-B^2}} \tag{1}$$

where F is a function of U, the 10m-elevation wind speed, r ~~, the particle radius~~ at relative humidity (RH) equal to 80%, and $B = \frac{(0.380 - logr)}{0.650}$. The source function is applied for particles with dry diameters of 0.45 μm or more (equivalent to model particle diameters). For particles with dry diameters less than 0.45 μm, a correction is applied based on reported data in *O'Dowd et al. (1997)*, since G97 overestimates the production of small particles *(Gong, 2003; De Leeuw et al., 2011)*. G97 is based on the whitecap method, where the emission flux scales linearly with the fraction of the ocean area covered by whitecaps. Over open ocean, the whitecap fraction, W(U), is determined as a function of wind speed (*Monahan and Muircheartaigh (1980)*; MO80 from now on):

$$W(U) = 3.84 \times 10^{-6} \times U_{10}^{3.41} \tag{2}$$

This expression for W(U) is included implicitly in Equation (1) following details provided in MO80. In the base version, SSA emissions are calculated for every grid cell, which is open ocean or salt-water lakes. In this study, the grid cell which is covered by sea-ice is considered and then the fraction of that ice-free grid is used. In this way, SSA emissions from open leads are taken into account. It can be noted that this SSA scheme, based on *Gong et al. (1997)*, is still being used in global and regional models (e.g. the Community Multiscale Air Quality Modeling System (CMAQ), *(Gantt et al., 2015)*, Goddard Earth Observing System (GEOS)-Chem, *(Huang and Jaeglé, 2017)*, or in other models (e.g. LOTUS-EUROS) *(Barthel et al., 2019)* to simulate SSA, despite being relatively old. However, modelling studies have shown that G97 overestimates super-micron SSA (e.g. ~~(Jaeglé et al., 2011)~~ *Jaeglé et al. (2011)*, JA11 from now on) or underestimates sub-micron SSA (e.g. *Archer-Nicholls et al. (2014); Gantt et al. (2015)*).

4.2 Updates to SSA emissions - HEM_NEW run

Here, updates to the model ~~treatments~~ treatment of SSA emissions are described. They are included in the run HEM_NEW, which is also used as boundary conditions for the higher resolution runs over northern Alaska.

4.2.1 Sub-micron SSA emissions including marine organics

Previous studies have shown that there are large numbers of SSA down to 10 nm *(Ovadnevaite et al., 2014; Cravigan et al., 2015; Xu et al., 2022)*. Also, data-based studies in the Arctic *(Kirpes et al., 2019),* and over the Atlantic Ocean *(O'Dowd et al., 2004; Ovadnevaite et al., 2011; Saliba et al., 2019)*~~suggested~~, suggest that marine organics associated with SSA contribute significantly to natural aerosol composition. Marine organics are not included in G97. However, *Archer-Nicholls et al. (2014)* implemented a scheme in the SSA emission module of MOSAIC based on *Fuentes et al. (2010, 2011)* (F10 and F11 from now on) to include a source flux for marine organics with dry diameters from 0.003 to 0.45 μm, that is coupled to G97 for larger particles. This scheme is activated in HEM_NEW simulations. F10 is applied from the lower aerosol bin, namely 39 nm. The scheme is based on an analysis of data from a mid-latitude cruise investigating the influence of dissolved OM on the production

270   of sub-micron SSA. The F10 SSA source function also depends on MO80 whitecap coverage and high wind speed dependence. Organic fractions equal to 0.2 for the first and second MOSAIC bins, 0.1 for the third bin and 0.01 for the remaining bins are used following the high biogenic activity scenario which assumes high C̶carbon (C):Chlorophyll-a (Chl-a) ratios (see *Lee et al. (2010)*). F11 found that higher particle organic fractions are expected in algal bloom regions with high C:Chl-a ratios and Chl-a varying between 0.4-10 μgL^{-1}. The use of the F11 high biogenic activity option is justified since MODIS-Aqua satellite

275   data (https://neo.sci.gsfc.nasa.gov/view.php?datasetId=MY1DMW_CHLORA&date=2014-12-01) for January-February 2014 s̶h̶o̶w̶ shows that Chl-a south of Alaska, and along the west coast of the United States, varied between 0.3 and 3.0 μgL^{-1}. *Fujiki et al. (2009)* also found that Chl-a varied between 0.4 and 1.0 μgL^{-1} at six stations south of the Aleutian Islands, Alaska, during a sub-Arctic cruise in autumn 2005. Details about the F10 SSA source function are given in APPENDIX B. Thus, in the HEM_NEW run, OA also includes marine organics. Possible regional sources of marine organics over northern Alaska are

280   discussed further in Section 6.

4.2.2   Wind speed dependence

As noted earlier, SSA emissions are highly dependent on wind speed and sea state (presence of whitecaps). The G97 scheme, and the related parameterisation by *Gong (2003)*, depend on the whitecap method and thus have a high wind speed dependence (see Eq. 1). Several studies have tried to improve upon the whitecap method. *Callaghan et al. (2008)* used an automated

285   whitecap extraction technique to derive two whitecap expressions that differ from MO80, and are based on cubed relationships for U_{10}. For sub-micron SSA, *Ovadnevaite et al. (2012)* showed that source functions, such as *Gong (2003)*, based on the MO80 wind speed dependence, are responsible for an overestimation of the SSA emission flux. They found a lower wind speed dependence for small particles, based on an autumn field study off the west coast of Ireland. Other factors, such as the wave field *(Salisbury et al., 2013)* or fetch-dependent threshold for breaking waves *(Revell et al., 2019; Hartery et al.,*

290   *2020)*, have also been shown to affect whitecap lifetime, with implications for SSA production. In a study by *Salisbury et al. (2014)* ,̶(SALI14 from now on),̱ satellite data from Quick Scatterometer (QuikSCAT) were used to derive an expression with a lower wind speed dependence compared to MO80. Here, the SALI14 parameterisation is implemented, instead of the MO80 whitecap fraction expression, since it is based on satellite data analysis providing information with global coverage including the Arctic (e.g. Chukchi Sea and Barents Sea during autumn) and south of Alaska:

295   $$W(U) = 4.60 \times 10^{-5} \times U_{10}^{2.26} \tag{3}$$

Based on Figure 2 in SALI14, the seasonal mean of $W(U_{10})$ using Eq. 3 is lower at latitudes above 40N and 40S compared to MO80 during autumn and winter.

4.2.3   SST dependence

Wind speed alone cannot predict SSA variability, and it is important to also include a dependence on SSTs as pointed out by,

300   for example, data-based studies in the Arctic *(Saliba et al., 2019; Liu et al., 2021b)* and mid-latitudes, such as *Ovadnevaite et al. (2014)*. Modelling studies also showed that the application of a SST dependence improves simulated SSA concentrations

compared to observations *(Jaeglé et al., 2011; Sofiev et al., 2011; Spada et al., 2013; Barthel et al., 2019)*, but not yet implemented in WRF-Chem. More specifically, previous studies tested different SSA source functions and reported that including a SST dependence improves model results, regardless of the wind speed dependence employed *(Spada et al., 2013; Grythe et al., 2014; Barthel et al., 2019)*. However, uncertainties still remain about the influence of SSTs on SSA production *(Revell et al., 2019)*, including the role of other factors, such as seawater composition *(Callaghan et al., 2014)* or wave characteristics (e.g. wave speed and breaking wave type, *Callaghan et al. (2012)*), which might be more important than SSTs alone. Here, the JA11 SST correction factor is applied when SSTs are between -2°C and 30°C to evaluate the effect of SSTs on sub- and super-micron SSA emissions. SSTs are provided by the reanalyses data, in this case, FNL, and in the presence of sea-ice, ~~SST is~~ SSTs are set equal to -1.75°C. In that case, the SST correction factor is set to the minimum value based on *Barthel et al. (2019)*.

~~Average absolute differences in super-micron aerosol mass concentrations (in μgm^{-3}) between HEM_NEW and CONTROL during January and February 2014 at the surface. The black x in northern Alaska shows where Utqiaġvik is located. The black circle shows Alert, Canada, the black diamond shows Villum in Greenland, while the black pentagon shows Zeppelin, Svalbard. Total SO$_4^{2-}$ is shown. All the results are shown north of 50N. Note the different scales.~~

4.2.4 Sea-salt sulphate

A source of ss-SO$_4^{2-}$ is included in the MOSAIC SSA emission scheme (HEM_NEW), since it was not included in the base model version (CONTROL). The mass fraction of ss-SO$_4^{2-}$ is estimated to be 0.252 of the Na$^+$ mass fraction based on *Kelly et al. (2010)* and *Neumann et al. (2016)*. The fraction of ss-SO$_4^{2-}$ is subtracted from the fraction of Na$^+$, Cl$^-$, and marine OA. Note that the total fraction of Na$^+$, Cl$^-$, marine OA, and ss-SO$_4^{2-}$ is equal to 1.0, and additional emissions are not added. We find that, on average, the mass fraction of ss-SO$_4^{2-}$ emissions in our simulations is around 9.9% of the total SSA emissions. This can be compared with the CMAQ model where the ss-SO$_4^{2-}$ emissions are estimated to be 7% of the total SSA emissions *(Kelly et al., 2010)*.

5 Evaluation of simulated wintertime SSA and other aerosols over the Arctic

First, absolute differences in simulated aerosol concentrations between the HEM_NEW and CONTROL results, averaged over January and February 2014, are presented. Model results from the two runs are then evaluated against available observations of, not only Na$^+$ and Cl$^-$, but also OA and SO$_4^{2-}$ which now include a sea-salt component, and NO$_3^-$ which is affected by heterogeneous reactions on SSA. We also show NH$_4^+$ for completeness. Lastly, we compare observation-based and modelled contributions of SSA to total wintertime inorganic aerosol concentrations during winter 2014.

5.1 SSA emission updates: HEM_NEW versus CONTROL

Average absolute differences in super-micron and sub-micron inorganic aerosols between the HEM_NEW and CONTROL are shown in Figures 2 and 3, respectively. HEM_NEW simulates less super-micron Na$^+$ by up to 20 μgm^{-3}, and Cl$^-$ by up to 30
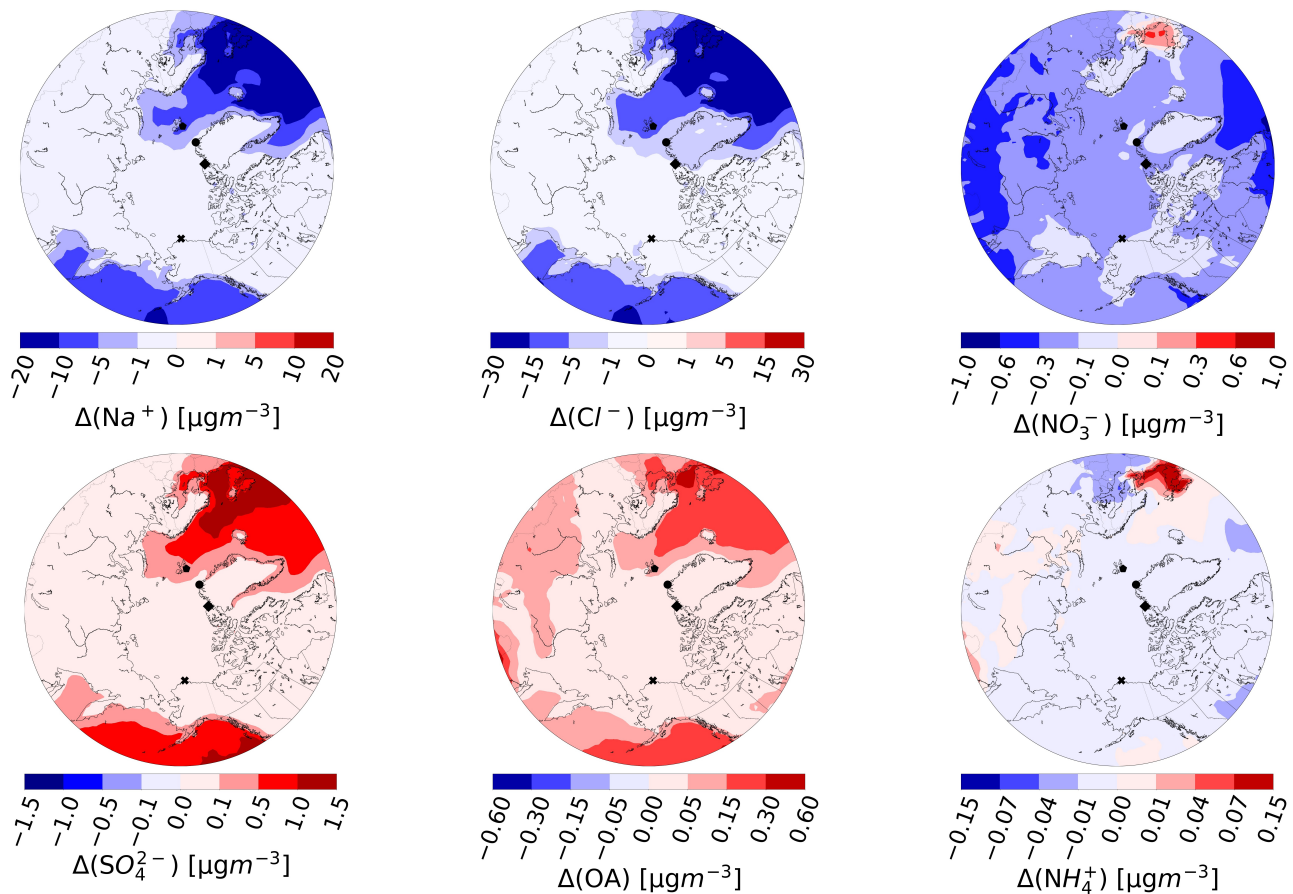
Figure 2. ~~The same as Figure 2, but for sub-micron~~ Average absolute differences in super-micron aerosol mass concentrations (in μgm^{-3}) between HEM_NEW and CONTROL during January and February 2014 at the surface. The black x in northern Alaska shows where Utqiaġvik is located. The black circle shows Villum in Greenland, the black diamond shows Alert, Canada, while the black pentagon shows Zeppelin, Svalbard. Total SO_4^{2-} is shown. All the results are shown north of 50N. Note the different scales.

μgm^{-3}, especially south of Alaska and the northern Atlantic Ocean. This is due to the combined effect of using a lower wind speed dependence and including the SST dependence (Fig. 2). Inclusion of a SST dependence leads to a larger decrease in locally produced super-micron Na^+ and Cl^- over the Arctic and sub-Arctic ice-free regions, due to lower temperatures north of 50N, compared to using the lower wind speed dependence, based on SAL14, which has a smaller effect. Overall, one-third of the super-micron reductions can be attributed to the lower wind speed dependence and two-thirds to the SST dependence. Super-micron NO_3^- is also lower (by up to 1.0 μgm^{-3}) due to less formation of NO_3^- via heterogeneous uptake of HNO_3 on SSA. These reactions involving heterogeneous uptake of acid gases also produce HCl, thus depleting Cl^- relative to Na^+ *(Su et al., 2022)*. The presence of sea-ice also plays a role. Smaller decreases in Na^+ and Cl^- are found north of Alaska (Beaufort Sea) compared to ice-free regions such as the northern Atlantic Ocean. The local influence of sea-ice fraction and open leads on

SSA production over northern Alaska are examined further in Section 6. Furthermore, due to the addition of marine organics and ss-SO_4^{2-} in HEM_NEW, there is more super-micron SO_4^{2-}, by up to 2 μgm^{-3}, and super-micron OA, by up to 0.6 μgm^{-3}, over marine regions. Super-micron NH_4^+ slightly increases up to 0.15 μgm^{-3} over regions where NO_3^- increases.
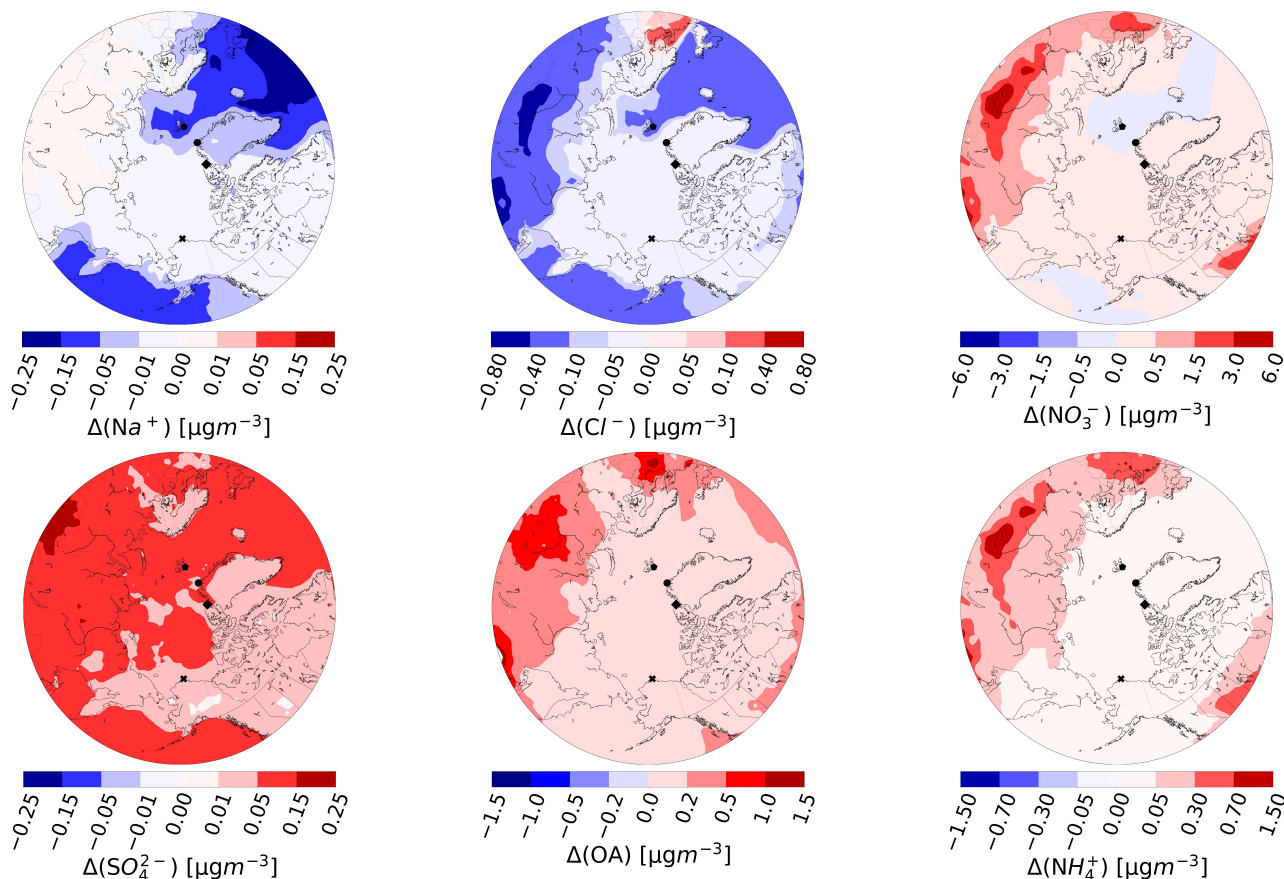
Figure 3. The same as Figure 2, but for sub-micron aerosol mass concentrations.

345   There are smaller decreases in HEM_NEW sub-micron Na^+ compared to CONTROL, by up to 0.25 μgm^{-3}, south of Alaska and in the North Atlantic (Fig. 3). Again, this is due primarily to the introduction of the SST dependence. When using SALI14 lower wind speed dependence alone, there is a small decrease in sub-micron Cl^- and a small increase in sub-micron Na^+ over the Arctic. Sub-micron Cl^- also decreases over continental areas, where NO_3^- and HNO_3 are higher due to anthropogenic sources (Fig. 3). Heterogeneous uptake on SSA reduces Cl^- and increases sub-micron NO_3^- by up to 6.0 μgm^{-3} in HEM_NEW

350   over continental regions while the increases over the Arctic Ocean are smaller. This is in contrast to super-micron NO_3^- decreases. These results are consistent with the study of *Chen et al. (2016)*, also using WRF-Chem with MOSAIC, who noted that since SSA are primarily present in the coarse (super-micron) mode, this favours the formation of $NaNO_3$ which is thermodynamically stable, and limits the formation of NH_4NO_3 which is semi-volatile *(Chen et al., 2020)*. Therefore, lower

Table 2. Biases in aerosol mass concentrations, in μgm^{-3}, averaged over January and February 2014 for the CONTROL and HEM_NEW simulations compared to the observations. NA stands for not available.

	CONTROL	HEM_NEW	CONTROL	HEM_NEW	CONTROL	HEM_NEW	CONTROL	HEM_NEW	CONTROL	HEM_NEW	CONTROL	HEM_NEW
	Na^+		Cl^-		NO_3^-		nss-SO_4^{2-}	nss-SO_4^{2-}/ ss-SO_4^{2-}	NH_4^+		OA	
Alert	0.81	0.12	1.05	-0.03	0.28	0.25	0.06	-0.02/ 0.04	0.011	0.01	NA	NA
Villum	1.3	0.27	1.9	0.27	0.25	0.14	0.05	0.04/ 0.07	0.01	0.01	NA	NA
Zeppelin	3.3	0.2	4.9	0.1	0.13	0.2	0.2	0.24/ 0.12	0.01	-0.01	NA	NA
Utqiaġvik super-micron	0.3	-0.07	0.27	-0.26	0.26	0.13	0.005	0.006/ -0.02	0.004	-0.001	NA	NA
Utqiaġvik sub-micron	-0.485	-0.489	-0.116	-0.124	-0.065	-0.054	-0.621	-0.47/ -0.12	0.11	-0.06	NA	NA
GoA	0.6	0.2	0.7	0.1	0.3	0.2	-0.04	-0.07/ 0.04	NA	NA	-0.24	-0.21
Simeonof	1.4	0.3	2.0	0.1	0.12	0.08	-0.2	0.05/ 0.09	NA	NA	-0.08	-0.05

super-micron SSA in HEM_NEW, results in less super-micron NO_3^- and more sub-micron NO_3^-. We also note that, for these reasons, sub-micron NH_4^+ also increases, by up to 1.5 μgm^{-3}, especially over continental areas, and displays similar regional patterns to sub-micron NO_3^-. Inclusion of marine organics linked to SSA, leads to increases in sub-micron OA, by up to 1.5 μgm^{-3}, and total SO_4^{2-} increases due to the addition of ss-SO_4^{2-}.

5.2 Evaluation against observations

Model results are evaluated against available observations of aerosols at different sites as shown in Figures 4, 5 and 6. These figures are grouped according to the size ranges of the measurements at the different sites as discussed in Section 3.1. Mean biases and root mean square errors (RMSEs) between the observations and the model results are given in Table 2 and Table C.1 (APPENDIX C), respectively. In the following the main findings are discussed by aerosol component.

SSA (Na^+ and Cl^-): Updates to the treatment of SSA emissions in HEM_NEW greatly improves modelled SSA over the Arctic with notable reductions in biases and RMSEs in Na^+ and Cl^- compared to observations at Alert, Zeppelin (d_a < 10 μm), Villum (TSP), Gates of the Arctic (GoA) (fine mode), and the sub-Arctic site, Simeonof (fine mode). Overall, HEM_NEW captures the spatial variability between the observed Na^+ and Cl^- at the different sites, in particular, the lower observed concentrations at Villum, which is surrounded by sea-ice at this time of year, and higher concentrations at Simeonof and Zeppelin. The extent to which sea-ice is present near different sites is an important factor. For example, the high variability in modelled SSA at Villum at the end of January and the middle of February 2014 is likely to be due to fluctuations in sea-ice fraction around the site (0.9-1.0 in the FNL analyses). At Utqiaġvik, the model captures super-micron Na^+, whereas Cl^- is now underestimated due to Cl^- depletion.

Sub-micron Na$^+$ and Cl$^-$ are still underestimated in HEM_NEW at this site with average biases of about -0.5 μgm^{-3} for Na$^+$ and -0.12 μgm^{-3} for Cl$^-$ with higher biases during episodes with elevated observed SSA. ~~Sub-micron SSA at this site~~ Here, sub-micron SSA may have been transported to the Arctic from the Pacific Ocean *(Quinn et al., 2002; May et al.,*

375 *2016)*, and thus model underestimations may point to deficiencies in the SSA source function further south or issues related either to long-range transport or to wet and dry deposition treatments in the model. However, the fact that the model agrees better with observations over the wider Arctic, as well as at sub-Arctic Simeonof, provides confidence in the modelled long-range transport as a source of Arctic (sub-micron) SSA. Simulated SSA also compares well with reported weekly averaged sub-micron Na$^+$ mass concentrations collected during January and February 2014 at Alert (0.1 μgm^{-3} observed, up to 0.08

380 μgm^{-3} modelled) *(Leaitch et al., 2018)*. We also note that, at Utqiaġvik, while *May et al. (2016)* attributed sub-micron SSA to long-range transport, KRP18 estimated that 42% of their analysed samples in the sub-micron range were fresh SSA with chemical signatures similar to sea-water, with 18% classed as partially aged with enhanced anthropogenic components (S, N) and depleted Cl$^-$, and the remainder included organics and sulphate particles. Thus, model discrepancies may also be due to local processes influencing SSA over northern Alaska. This is investigated further in Section 6.

385 **Nitrate**: Improved SSA treatments in HEM_NEW also lead to improved simulation of NO$_3^-$ at some sites, notably Simeonof, GoA, Alert, Villum, and biases are reduced (see Table 2). While modelled super-micron NO$_3^-$ at Utqiaġvik is improved, the model still underestimates certain periods when elevated sub-micron NO$_3^-$ is observed, also the case at GoA and Simeonof. The improved behaviour of modelled NO$_3^-$ is, in general, due to reductions in Na$^+$ and Cl$^-$, leading to less NO$_3^-$ production in the coarse mode, especially close to or just downwind of major anthropogenic emission regions at mid-latitudes, and a shift to more

390 NO$_3^-$ in the fine mode, as discussed previously. These effects are most evident at Utqiaġvik, where the model can be compared to sub- and super-micron data. Comparison with data from other sites is with either total, coarse plus fine mode, or fine mode aerosol observations, and therefore includes both increases and decreases in simulated NO$_3^-$. Overall, these results illustrate the importance of correctly simulating SSA and its effects on anthropogenic aerosols. While observed NO$_3^-$ concentrations are generally lower than other aerosol components, such as Na$^+$, Cl$^-$ or nss-SO$_4^{2-}$, during Arctic winter, a recent trend analysis

395 study showed that NO$_3^-$ is clearly increasing at Alert, especially during the winter months *(Schmale et al., 2022)*. Such increases in NO$_3^-$ may be due to increased NO$_3^-$ formation due to lower acidity following SO$_2$ reductions, that outweigh reductions in NO$_x$ emissions at mid-latitudes *(Sharma et al., 2019)*. However, increases in SSA over the Arctic Ocean, due to reductions in ice-covered waters, may also explain these changes (e.g. *Browse et al. (2014)*) although no significant trends in Na$^+$ have yet been detected *(Schmale et al., 2022)*.

400 **Sulphate**: Figures 4, 5 and 6 show observed ss-SO$_4^{2-}$ and total-SO$_4^{2-}$ together with results from CONTROL and HEM_NEW. With regard to total simulated SO$_4^{2-}$, the addition of ss-SO$_4^{2-}$ improves the model results, for example, at Simeonof where observed fine mode ss-SO$_4^{2-}$ makes a significant contribution (30-80%, up to 0.3 μgm^{-3}) to total SO$_4^{2-}$. ss-SO$_4^{2-}$ also contributes between 10-40% of total SO$_4^{2-}$ at Alert and Villum and modelled ss-SO$_4^{2-}$ agrees better with the observations. The remainder is nss-SO$_4^{2-}$, a dominant component of Arctic Haze resulting from long-range transport from sources in Russia and Europe

405 at these sites *(Leaitch et al., 2018; Lange et al., 2018)*. Model results are at the lower end (up to 0.3 μgm^{-3}) of reported sub-micron nss-SO$_4^{2-}$ mass concentrations (0.3-1.1 μgm^{-3}) at Alert during winter 2014 *(Leaitch et al., 2018)*. On the other hand,
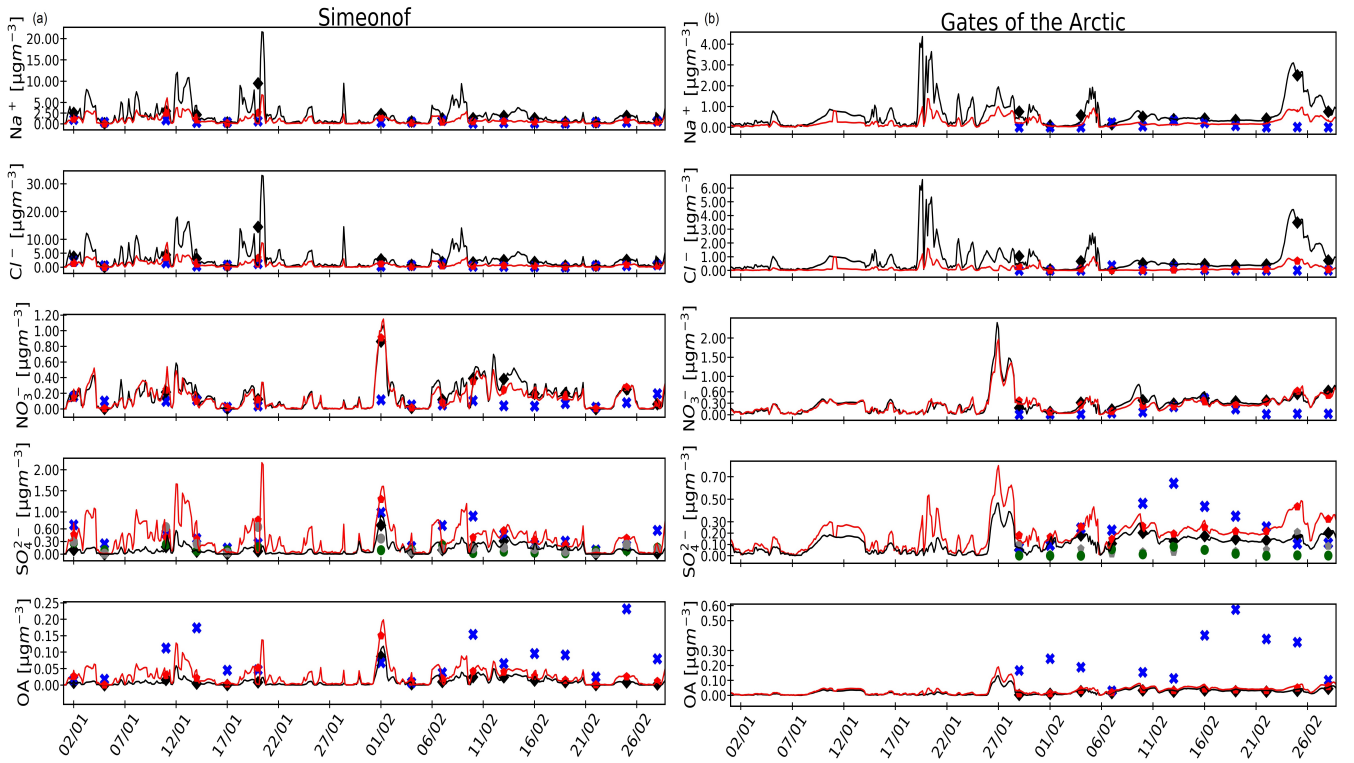
Figure 4. Evaluation of modelled aerosol composition against in-situ fine mode aerosol observations (both sites) at (a) Simeonof, Aleutians Islands, Alaska and (b) GoA, north of Alaska, in local Alaskan time (AKST). Observations are shown as blue crosses, only when they are available. For observed SO_4^{2-}: dark-green circles show ss-SO_4^{2-}, while blue crosses are total SO_4^{2-}. The black line shows model results from the CONTROL run; the red line shows results from the HEM_NEW run. Model daily or weekly averages are shown as black diamonds for CONTROL and red pentagons for HEM_NEW, while grey circles show ss-SO_4^{2-} for from the HEM_NEW simulation. See the text for more details. Note the different scales.

HEM_NEW further overestimates total observed SO_4^{2-} at Zeppelin due to the inclusion of ss-SO_4^{2-}, especially during certain episodes with elevated concentrations. We note that Zeppelin is a mountain site at 471m, and thus discrepancies with the observations may also be due to issues simulating the vertical distribution and transport of nss-SO_4^{2-} from Eurasian source regions

410 *(Hirdman et al., 2010).* At Utqiaġvik, on the northern coast of Alaska, most of total observed super-micron SO_4^{2-} is ss-SO_4^{2-} (up to 0.18 μgm^{-3}, around 80%), and the inclusion of ss-SO_4^{2-} in HEM_NEW improves agreement with the observations. With regard to total sub-micron SO_4^{2-}, high mass concentrations are observed at Utqiaġvik compared to other Arctic sites, consisting mostly of nss-SO_4^{2-}, peaking at 2.4 μgm^{-3}, much higher than total super-micron SO_4^{2-} (peaking at 0.5 μgm^{-3}), as also reported by *Quinn et al. (2002).* However, the model underestimates nss-SO_4^{2-} at this site. As noted by KRP18 and KRP19, this is

415 likely to be due to the there is a local influence from the North Slope of Alaska (NSA) oil fields to the east, and these emissions may be underestimated in the model. In a companion paper , Ioannidis et al. (2022, in prep.) the influence of these regional
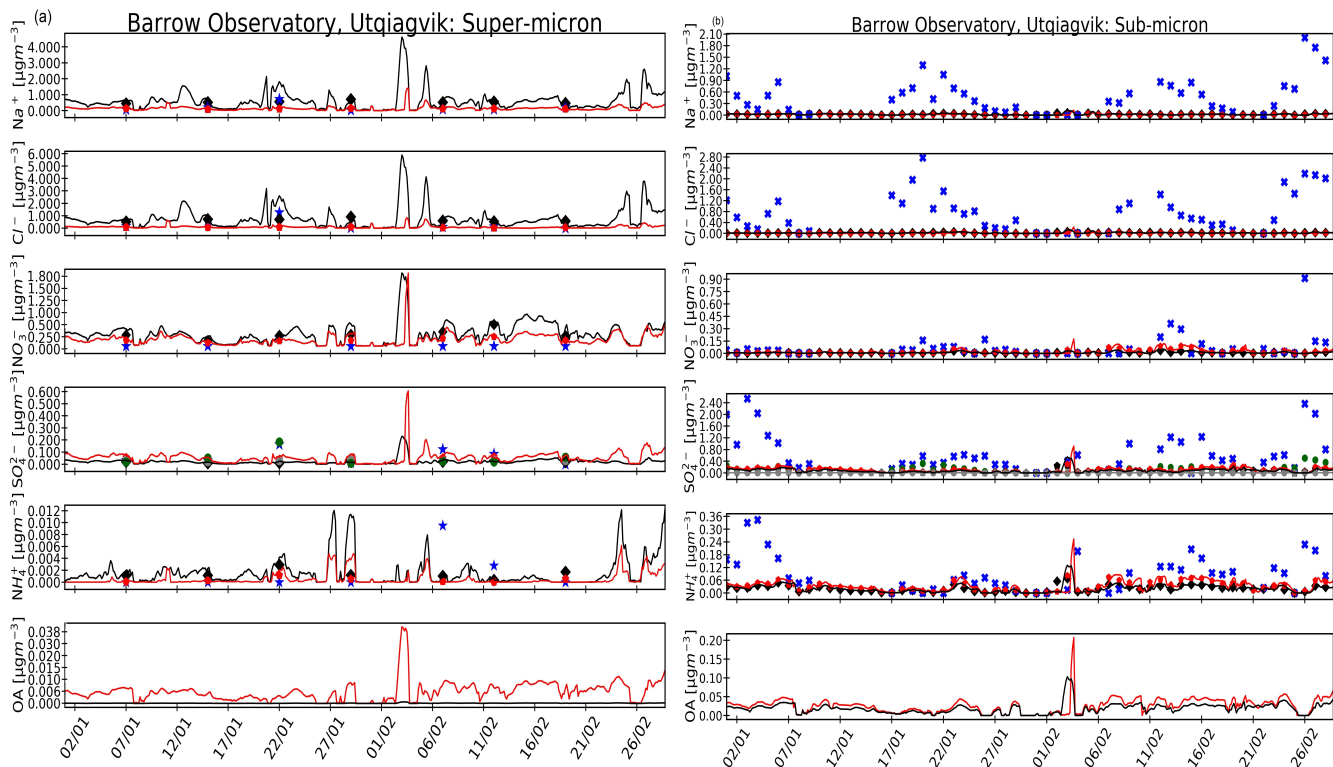
Figure 5. Evaluation of modelled aerosol composition against observations at Utqiaġvik for (a) super-micron and (b) sub-micron in Coordinated Universal Time (UTC) and in standard temperature pressure (STP) conditions. Observations are shown only when available. The lines and the symbols are the same as in Figure 4. See the text for more details. Note the different scales.

emissions on BC at Barrow is investigated during winter 2014 finding investigating BC at Utqiaġvik, it is estimated that up to 30-50% of BC may originate from this source originates from these regional emissions *(Ioannidis et al. 2023 in prep.)*. Indeed, at GoA, 391km inland from the coast, and south of the NSA oil fields, the contribution of nss-SO_4^{2-} is more important and ss-SO_4^{2-} is negligible. The Here, the model captures total fine mode SO_4^{2-} (peaking up to 0.64 μgm^{-3}) at this site and the addition of ss-SO_4^{2-} does not affect the results. As well as In addition to local sources, model difficulties simulating sub-micron nss-SO_4^{2-} at Utqiaġvik may be due to underestimation in transport of mid-latitude sources an underestimation in the transport of nss-SO_4^{2-} from mid-latitudes to the Arctic or issues related to deposition (as noted earlier for SSA), as also discussed in previous studies such as *Whaley et al. (2022)*. SO_4^{2-} formation mechanisms under dark, cold winter conditions may also be lacking in the model. For example, high concentrations of hydroxymethane sulphonate (HMS) have been measured recently during winter in Fairbanks, Alaskan Interior *(Campbell et al., 2022)* contributing to secondary SO_4^{2-} formation during Arctic winter, although only a small contribution from HMS to SO_4^{2-} was found in observations at Oliktok Point, situated within NSA oil fields *(Liu et al., 2021a)*. Oxidation of SO_2 by ozone (O_3) in alkaline SSA could also contribute up to 9% to SO_4^{2-}

formation *(Alexander et al., 2005)*. However, the version of WRF-Chem used here does not include such reactions, in common
430 with many chemistry-aerosol models run over the Arctic *(Whaley et al., 2022)*.

Ammonium: NH_4^+ observations are available at all sites except for Simeonof and GoA. Observed NH_4^+ concentrations are very low (below 0.2 μgm^{-3}) at Alert and Villlum, with higher concentrations observed at Zeppelin. Overall there is a good agreement between the model and measurements, with very low biases and RMSEs in both runs, apart from an underestimation of elevated NH_4^+ at Zeppelin. At Utqiaġvik, there is good agreement with super-micron NH_4^+, except for periods with higher
435 observed NH_4^+ (up to 0.1 μgm^{-3}). However, the model underestimates periods with elevated sub-micron NH_4^+, of up to 0.4
μgm^{-3}, which is higher compared to the other sites. Temporal variations in NH_4^+ during January and February 2014, generally, follow nss-SO_4^{2-} as NH_4^+ preferentially forms ammonium bisulfate and, to a lesser extent, ammonium sulfate in the particle phase *(Schmale et al., 2022)*, and they have common anthropogenic origins. Previous studies also noted that NH_4^+ is two times higher at Utqiaġvik than at Alert, Zeppelin and Villum, while SO_4^{2-} concentrations are similar at all three ~~stations~~ sites
440 *(Schmale et al., 2022)*, possibly suggesting differences in aerosol acidity at different sites. This is also found in this study based on the observations and ~~modelled~~ model results (HEM_NEW). It is therefore interesting to investigate the effect of the improved SSA emissions on modelled aerosol acidity. For this, we estimate the neutralisation factor f, following *Fisher et al. (2011)*. The results are discussed in APPENDIX D. CONTROL tends to predict more acidic aerosols than observed. Based on the observations, most acidic aerosols are found at Alert, Zeppelin and Utqiaġvik (super-micron), with somewhat less acidic
445 aerosols at Villum and Utqiaġvik (sub-micron). This is improved to some degree in HEM_NEW with aerosols becoming less acidic at some sites, notably at Alert and Villum, due to decreases in simulated NO_3^-. However, modelled sub-micron aerosols at Utqiaġvik are less acidic than the observations, due to the underestimation of nss-SO_4^{2-}. Overall, the updates to SSA emissions lead to somewhat less acidic anthropogenic aerosols over the Arctic, again highlighting the importance of interactions between SSA and other inorganic aerosols.

450 **Organic aerosols**: Only two sites provide tOC fine-mode observations ranging from between 0.15-0.3 μgm^{-3} at Simeonof and 0.15~~and 0.5~~ -0.5 μgm^{-3} at GoA during January and February 2014. The inclusion of marine organics in HEM_NEW improves modelled OA, especially at the coastal Simeonof site. Since observations at other sites are not available for winter 2014, results are compared with other reported measurements. *Shaw et al. (2010)* reported sub-micron OA at Utqiaġvik ~~equal to~~ around 0.3 μgm^{-3} during winter 2008 (November to February). However, a more recent study by *Moschos et al. (2022a)*
455 reported lower wintertime OA concentrations ($d_a < 10$ μm) at this site (around 0.1 μgm^{-3}), attributed mostly to primary-anthropogenic or ~~haze~~ Haze OA originating from Eurasia. However, modelled OA for the same size range is only up to 0.05 μgm^{-3}. At Villum, *Nielsen et al. (2019)* also reported higher sub-micron OA observations, peaking at 2.2 μgm^{-3} in February 2015, attributed mostly to Arctic Haze influence (up to 1.1 μgm^{-3}) with secondary influences from hydrocarbon-like organics (up to 1.0 μgm^{-3}) and marine sources (up to 0.2 μgm^{-3}). Modelled OA in HEM_NEW at this site does not exceed 0.1 μgm^{-3}.
460 Overall, the model underestimates Arctic OA in common with many other models *(Whaley et al., 2022)*. These discrepancies may be due missing or underestimated anthropogenic or natural sources. For example, it is known that there are large uncertainties in anthropogenic OA emissions *(Marelle et al., 2017)*. The possibility of a wintertime marine OA source over northern Alaska is explored further in Section 6.
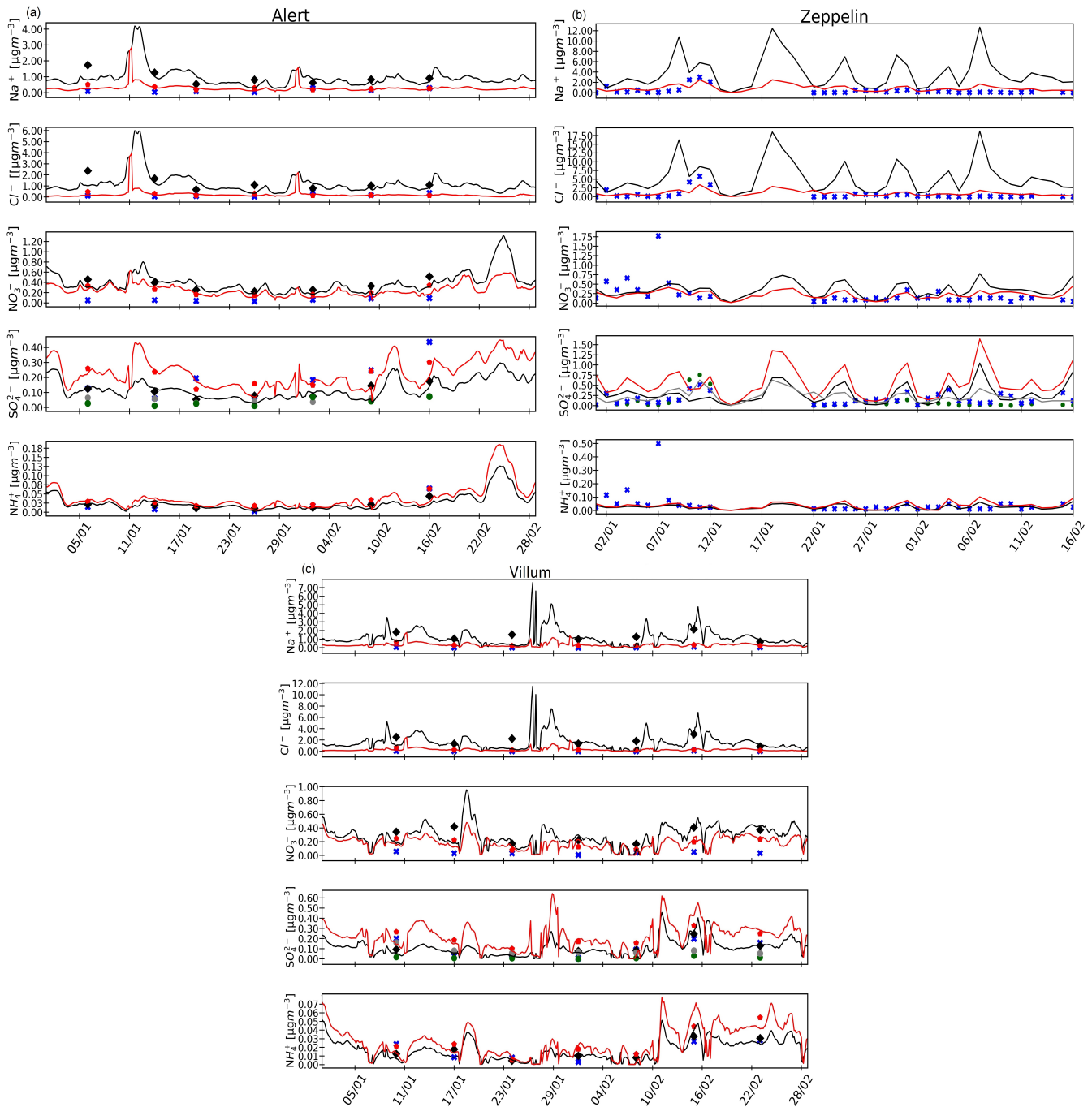
Figure 6. Evaluation of modelled aerosol composition against in-situ aerosol observations with $d_a < 10\ \mu$m ~~at~~ (a) ~~at~~ Alert, Canada (~~standard temperature pressure (~~STP ~~)~~ conditions), (b) ~~at~~ Zeppelin, Svalbard, and (c) TSP aerosols at Villum, Greenland in UTC. Observations are shown only when available. The lines and the symbols are the same as in Figure 4. See the text for more details. Note the different scales.

Table 3. Calculated fractions of observed and modelled (HEM_NEW) SSA to total inorganic aerosol mass concentrations. For each site, SSA are defined as the sum of Na^+, Cl^- and ss-SO_4^{2-}. Total is defined as the sum of SSA and inorganic aerosols. Inorganic is the sum of nss-SO_4^{2-}, NH_4^+ and NO_3^- for each ~~station~~ site except for Simeonof and GoA where inorganic is the sum of nss-SO_4^{2-} and NO_3^-. Total_all below is defined as the sum of SSA, nss-SO_4^{2-}, NH_4^+, NO_3^-, BC, OA and dust (model only). The aerosol size range for SSA, Total and Total_all varies per ~~station~~ site and corresponds to observed aerosol sizes as described in Section 3.

Sites	SSA/Total [obs]	SSA/Total [HEM_NEW]	SSA/Total_all [HEM_NEW]
Simeonof (fine mode)	0.73	0.84	0.74
GoA (fine mode)	0.20	0.44	0.33
Utqiaġvik-sub-micron	0.60	0.22	0.13
Utqiaġvik-super-micron	0.93	0.57	0.54
Alert (coarse mode)	0.59	0.54	0.45
Villum (TSP)	0.32	0.63	0.52
Zeppelin (coarse mode)	0.56	0.75	0.62

5.3 Contribution of SSA to total inorganic aerosols

465 Lastly, we assess the contribution of SSA to total inorganic aerosols in the Arctic during wintertime since previous studies noted that they can make an important contribution to total sub-micron and super-micron mass fractions at this time of year *(Quinn et al., 2002; May et al., 2016; Kirpes et al., 2018, 2019). Moschos et al. (2022b)* also showed SSA dominates wintertime PM_{10} (particulate matter with $d_a \leq 10\ \mu m$) mass concentrations at remote Arctic sites, including Alert (56%), Baranova (northern Russia) (41%)~~(Russia)~~, Utqiaġvik (66%), Villum (32%), and Zeppelin (65%). In contrast, at sites such as Tiksi

470 (northern Russia) and Pallas (Finland), SO_4^{2-} and OA dominate (70% and 55%, respectively). To investigate the contribution of SSA to total mass concentrations during the period of this study, observed and modelled fractions of SSA to "total" (SSA plus inorganic) aerosols are estimated (see Table 3). It should be noted that this fraction varies between sites since not all components were measured. Taking into account the observations available at each site, the fraction of SSA to total SSA plus inorganics is higher at all the coastal sites (Utqiaġvik, Alert, Simeonof, Villum) and Zeppelin ranging from 54 to 93%.

475 Only at the GoA and Villum is the fraction of SSA smaller (20% and 32%, respectively). SSA fractions, calculated using the HEM_NEW results, show similar patterns compared to the observations with fractions ranging between 44% and 84%. An exception, is Utqiaġvik where the modelled fraction is lower than in the observations due to low simulated sub-micron SSA concentrations. When taking into account all aerosol components in the model, including OA, BC and dust, SSA is dominant at Simeonof, Utqiaġvik (super-micron), Zeppelin and Villum (more than 54%), whereas at Alert, SSA contributes about 45%.

480 This analysis shows that SSA is an important fraction of total inorganic aerosols at most Arctic coastal sites during wintertime.

Overall, the results presented here show that the simulation of Arctic SSA, and other inorganic and organic aerosols, is improved as a result of the updated SSA emission treatments. In particular, simulated aerosols, including the coarse mode or super-micron fraction, are improved compared to the observations. The results also show that it is important to include natural

SSA emissions of ss-SO_4^{2-} and marine organics, although the latter are highly uncertain. Missing anthropogenic sources
could also be contributing underestimation of OA and nss-SO_4^{2-}. Many models in the recent AMAP model evaluation of
Arctic composition also showed similar discrepancies, attributed to issues with anthropogenic emissions, or model transport,
deposition and aerosol formation *(Whaley et al., 2022)*. The results presented here also confirm the importance of interactions
between SSA and other inorganic aerosols via heterogeneous uptake, affecting mass concentrations and size distributions,
notably NO_3^-, and thus model ability to capture wintertime Arctic Haze.

=1cm Description of the regional-scale WRF-Chem model simulations at 20km resolution over northern Alaska. See text for details. Simulation Name Description ALASKA_CONTROL_JAN HEM_NEW run at 20km, 23-28 January 2014 NEW_ALASKA_JAN including regional updates as in NEW_ALASKA_FEB ALASKA_CONTROL_FEB HEM_NEW run at 20km, 24-28 February 2014 LOC_ORG_FEB + Local source marine organics *(Kirpes et al., 2019)* SSA_WS_DEP_FEB + Sub-micron SSA wind-speed dependence *(Russell et al., 2010)* NEW_ALASKA_FEB + ERA5 sea-ice fraction (all regional updates)

6 Regional processes influencing SSA over northern Alaska

Possible processes affecting SSA emissions emissions of SSA on a regional scale over northern Alaska are now examined in
more detail, and in particular, those which may explain low modelled sub-micron SSA at Utqiaġvik. Model simulations are
run at 20km over northern Alaska for shorter periods in January and February 2014 corresponding to the KRP18 measurement
campaign. The boundary and initial conditions are taken from HEM_NEW. The sensitivity of modelled SSA to a local source
of marine organic aerosols, wind speed dependence, and the representation of sea-ice fraction is investigated (see Table 4 for
details about the simulations). Differences between runs with and without specific sensitivity tests are examined sequentially
for the February period, before evaluating a run including the main changes against observations at Utqiaġvik during the
January and February campaign periods. The possible role of blowing snow and frost flowers is also addressed.

=1cm
Table 4. Average absolute differences between LOC_ORG_FEB and ALASKA_CONTROL_FEB during Description of the February campaign for sub-micron Na^+, OA, NO_3^- (μgm^{-3}). All the results are shown regional-scale WRF-Chem model simulations at the surface 20km resolution over northern Alaska. See text and Table 4 for more details. Utqiaġvik is shown by the black dot. Note the different scales.

Simulation Name	Description
Regional simulations [20km]	
ALASKA_CONTROL_JAN	HEM_NEW run at 20km, 23-28 January 2014
NEW_ALASKA_JAN	including regional updates as in NEW_ALASKA_FEB
ALASKA_CONTROL_FEB	HEM_NEW run at 20km, 24-28 February 2014
LOC_ORG_FEB	+ Local source marine organics *(Kirpes et al., 2019)*
SSA_WS_DEP_FEB	+ Sub-micron SSA wind-speed dependence *(Russell et al., 2010)*
NEW_ALASKA_FEB	+ ERA5 sea-ice fraction (all regional updates)

6.1 Local source of marine organics

The F10 parametrisation used in the 100km HEM_NEW run is based on C:Chl-a from a cruise at mid-latitudes. Whilst phytoplankton blooms may not be expected in the high Arctic winter, previous studies have shown evidence of sea ice biological activity under low light conditions coupled with decreased sea ice in the Arctic *(Krembs et al., 2002; Lovejoy C., 2007; Hancke et al., 2018)* *(Krembs et al., 2002; Lovejoy et al., 2007; Hancke et al., 2018)*. Analysis of data collected over the Arctic and North Atlantic during winter, and the winter-spring transition, also showed that the majority of sub-micron OM is highly correlated with Na^+ concentrations *(Russell et al., 2010; Shaw et al., 2010; Frossard et al., 2011; Leaitch et al., 2018)*. More specifically, *Russell et al. (2010)* (RUS10 from now on) analysed samples from the International Chemistry Experiment in the Arctic Lower Troposphere (ICEALOT) cruise and found that most OM in the North Atlantic and the Arctic is composed of carbohydrate-like compounds containing organic hydroxyl groups from primary ocean emissions. *Frossard et al. (2014)* (FRSS14 from now on) investigated the sources and composition of atmospheric marine aerosol particles based on the analysis of various samples, including ICEALOT, reporting that ocean-derived organic particles include primary marine OA. In particular, they calculated the ratio of $OC:Na^+$ as a metric for comparing the composition of model-generated primary marine aerosol and seawater, and reported $OC:Na^+$ ratios of 0.45 in atmospheric marine aerosol particles. KRP19 also reported that, during their campaign in 2014, almost all individual SSA had thick organic coatings made up of marine saccharides with average C:Na mole ratios of 0.5 and 0.3 for sub-micron and super-micron SSA, respectively. They also identified open sea-ice leads, enriched with exopolymeric substances, as contributing to OA in winter SSA. Here, elemental fractions for sub- and super-micron aerosols, sampled during the KRP19 campaign, are used to better constrain modelled marine OC emissions. The ratio of sub- and super-micron $OC:Na^+$ is calculated, following FRSS14, and using the elemental fractions from KRP19, as an indicator of the presence of a local source of marine organics. The organic fraction of SSA emissions in WRF-Chem is increased from 0.2 to 0.4 for sub-micron (1st and 2nd MOSAIC bins), from 0.1 to 0.4 for the 3rd MOSAIC bin and from 0.01 to 0.11 for the remaining MOSAIC bins. Note again that no additional SSA mass is added.

Figure 7 shows the sensitivity of the model results to including a larger marine organic fraction over the regional domain. Sub-micron OA concentrations increase by a small amount, by up to 0.009 μgm^{-3}, especially south-west of Alaska and along coastal areas, including around Utqiaġvik. There are only two available daily observations at GoA during the February simulation period to evaluate the model results. The model captures better observed tOC at the end of February in the run (LOC_ORG_FEB) with higher organic fractions (not shown here). However, it underestimates tOC on 25 February when the observed tOC reached 0.33 μgm^{-3}. As mentioned previously, this discrepancy could also be due to missing local anthropogenic OA sources. Higher OA fractions in the super-micron leads to lower Na^+ and, as result lower NO_3^-. As indicated above in Section 5, a decrease in super-micron NO_3^- results in an increase in sub-micron NO_3^-. Sub-micron Na^+ increases probably due to the formation of $NaNO_3$ in the model. In the following runs, higher organic fractions are used instead of those from F10.

Average differences in mass concentrations of (a) sub-micron Na^+, OA, NO_3^-, in μgm^{-3} between SSA_WS_DEP_FEB and LOC_ORG_FEB. (b) The map on the left shows the average value of SSA emission fluxes in $\mu gm^{-2}s^{-1}$ during the February
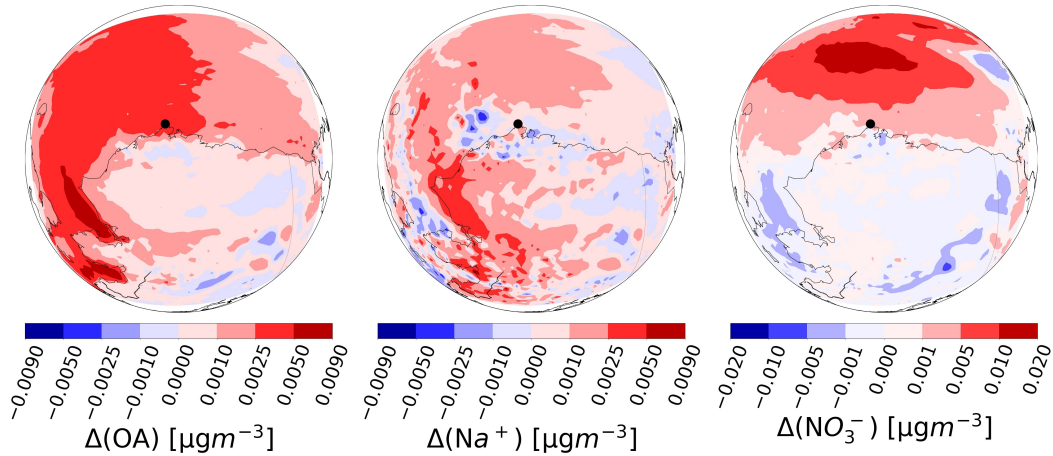
Figure 7. Average absolute differences in mass concentrations between LOC_ORG_FEB and ALASKA_CONTROL_FEB during the February campaign for sub-micron Na$^+$, OA, NO$_3^-$ (μgm^{-3}). All the results are shown at the surface. See text and Table 4 for more details. Utqiaġvik is shown by the black dot. Note the different scales.

~~campaign and the map on the right shows the average differences between SSA_WS_DEP_FEB and LOC_ORG_FEB emission fluxes in μgm^{-2}s^{-1}. All the results are shown at the surface. Utqiaġvik is shown by the black dot. Note the different scales.~~

6.2 Wind-speed dependence

540 In the 100km HEM_NEW run, a lower wind speed dependence based on satellite data ~~was~~ is used since it improves modelled SSA compared to observations at many sites over the Arctic as discussed in Section 5. However, RUS10 found evidence for higher wind speed dependence in the Arctic based on data collected during the Arctic leg of the ICEALOT cruise. They found that wind speed is a good predictor of a marine factor, calculated using positive matrix factorization, for sub-micron organic matter (OM1$_{sea}$). Their analysis showed a high correlation between OM1$_{sea}$, sub-micron sodium (Na$^+$1) and wind speed at

545 18m (correlation r equal to 0.90 for the North Atlantic and Arctic region, see Table S3 Supplementary Material in RUS10). Average OM1$_{sea}$ concentrations (0.2 μgm^{-3}) reported by RUS10 for the eastern Arctic Ocean are about half those reported at Utqiaġvik, for example, by *Shaw et al. (2010)* during wintertime.

In a sensitivity run, results from RUS10 are used to include a higher wind speed dependence for sub-micron SSA. This linear dependence differs from the power dependencies included in G97, SAL14, and other studies, but is based on empirical

550 relationships determined from analysis of data collected in the Arctic. Equations (5) and (6) from the RUS10 analysis for the Arctic legs of their cruise are applied to the model as a correction factor:

$$\text{Na}^+1 = 0.022 \times \text{U}_{18} - 0.012 \tag{4}$$
$$\text{OM1}_{sea} = 0.025 \times \text{U}_{18} - 0.049 \tag{5}$$
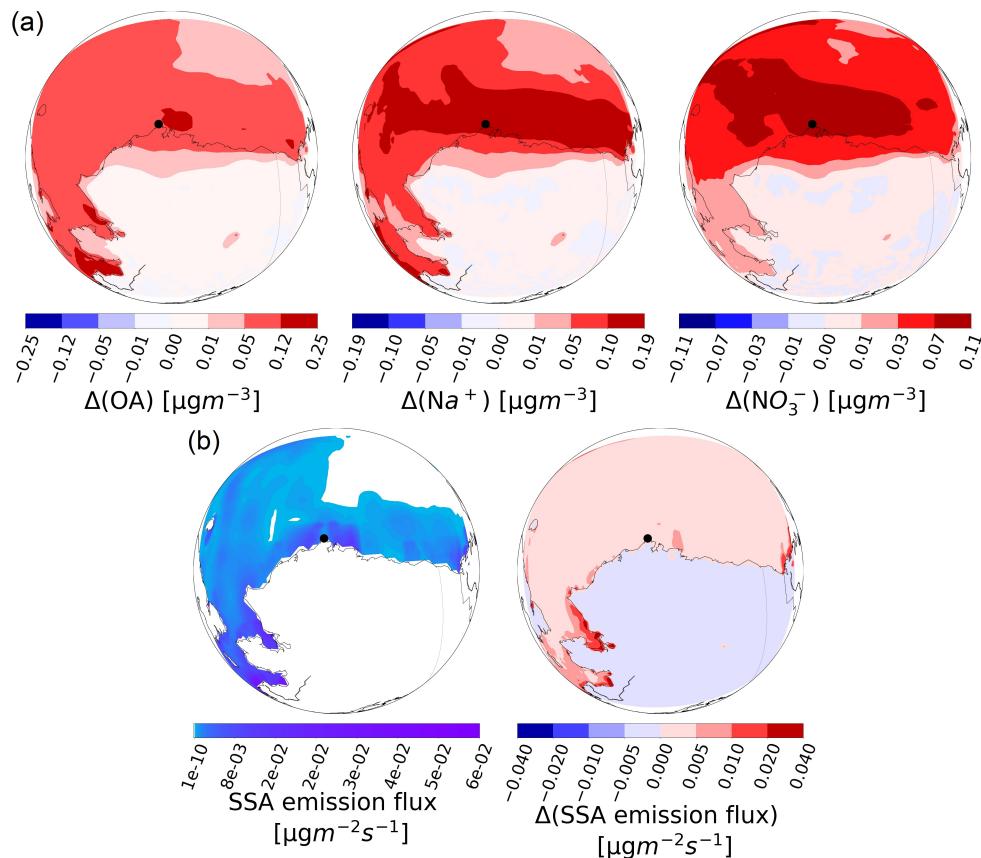
Figure 8. Average absolute differences in mass concentrations of (a) sub-micron Na^+, OA, NO_3^-, in μgm^{-3} between SSA_WS_DEP_FEB and LOC_ORG_FEB. (b) The map on the left shows the average value of SSA emission fluxes in $\mu gm^{-2}s^{-1}$ during the February campaign and the map on the right shows the average differences between SSA_WS_DEP_FEB and LOC_ORG_FEB emission fluxes in $\mu gm^{-2}s^{-1}$. All the results are shown at the surface. Utqiaġvik is shown by the black dot. Note the different scales.

where U_{18} is wind speed at 18m in ms^{-1}, for wind speeds between 2 and 14 ms^{-1} (Figure 2, RUS10). RUS10 used Na^+1
555 as a proxy for sub-micron NaCl, and subsequently SSA, because Na^+1 equalled sub-micron Cl^-1 on a molar basis for the North Atlantic and Arctic sampling regions. Thus, Equation (5) is also used to estimate a correction factor for Cl^-. Here, wind speeds in the first model layer are used, i.e. around 26m. Differences in U_{18m} and U_{26m} reach a maximum of 1 ms^{-1} (see Fig.E1 in APPENDIX E). Comparisons with radiosonde data at Utqiaġvik shows that the model performs well in terms of winds and temperatures (see APPENDIX E) and the role of meteorology on aerosols is not discussed further here. The correction factors
560 are only applied to simulated number and mass of the SSA emissions when modelled wind speeds are between 2 and 14 ms^{-1}, and when RUS10-calculated sub-micron SSA emissions are greater than model calculated SSA. In this way, SSA emissions are enhanced during periods ~~of~~ with higher wind speeds.

To illustrate the sensitivity of the results to applying this correction, Fig. 8 shows differences in sub-micron aerosol mass concentrations compared to the run including local marine organics, as well as model SSA emission fluxes, the latter being the sum of dry mass emissions calculated in the model. The SSA emission flux is affected over ice-free model grids leading to increased SSA production east and west of Utqiaġvik (by up to 0.015 μgm^{-2}s^{-1}) while the highest increases are southwest of Alaska (by up to 0.035 μgm^{-2}). This results in an increase of 0.25, 0.19 and 0.11 μgm^{-3} in sub-micron Na$^+$, NO$_3^-$ and OA, respectively, over the Utqiaġvik region and southwest Alaska during the February campaign. These results further illustrate the sensitivity of SSA emissions to wind speeds, in this case affecting fine mode aerosols. These results are in contrast to previous studies finding stronger wind speed dependencies for larger SSA particles, such as *Liu et al. (2021b)* who analysed aircraft data, including over the Arctic. However, size dependent source functions need to be developed for the Arctic region.

Average differences between ALASKA_NEW_FEB and SSA_WS_DEP_FEB showing the effect of switching from FNL to ERA5 sea-ice fractions during the February campaign for (a) SSA emission flux (μgm^{-2}s^{-1}), (b) sub-micron Na$^+$ and (c) super-micron Na$^+$ mass concentrations in μgm^{-3}. All the results are shown at the surface. Utqiaġvik is shown by the black dot. Note the different scales.

6.3 Sea-ice fractions

The sensitivity of modelled SSA to prescribed sea-ice fractions during wintertime and the role of leads, is also investigated since KRP19 already pointed out the importance of using realistic sea-ice distributions to simulate marine aerosols. High spatial resolution images of sea-ice cover are available, including during the polar night, from a radar operating on top of a building in Utqiaġvik town (71°17'13" N, 156°47'17" W), 22.5m above sea level, with a range of up to 11km to the northwest *(Druckenmiller et al., 2009; Eicken et al., 2011)*. *May et al. (2016)* previously showed increased super-micron Na$^+$ mass concentrations during periods of elevated wind speeds and lead presence, in a multi-year study using the sea ice radar data at Utqiaġvik. Between 23-28 January 2014, when the winds at Utqiaġvik were easterly, the radar showed that the coastal area east of Utqiaġvik featured open leads (KRP19). From 24-28 February 2014, the west coastal area also featured leads as also shown by Moderate Resolution Imaging Spectroradiometer (MODIS) satellite images (KRP19). To examine the sensitivity of modelled SSA emissions to sea-ice cover, ERA5 sea-ice fractions with a resolution of 0.25º x 0.25º are used instead of FNL fraction at 1.0º x 1.0º resolution. Note that only sea-ice fraction field is different, while the rest of the meteorological fields are from FNL.

Results for February are shown in Fig. 9. The SSA emission flux (Fig. 9a) increases over a small region west of Utqiaġvik and across the North Slope of Alaska due to decreased sea-ice fraction, but decreases just to the east of Utqiaġvik and southwest of Alaska due to increased sea-ice fraction. Sub-micron Na$^+$ slightly increases along the north coast of Alaska and around Utqiaġvik, by up to 0.1 μgm^{-3} (see Fig. 9b). Larger super-micron Na$^+$ are simulated by up to 0.4 μgm^{-3} around Utqiaġvik, and decreases by up to 0.4 μgm^{-3} southwest of Alaska (Fig. 9c). Higher SSA emission fluxes are simulated for February (0.035 μgm^{-2}s^{-1}) compared to January (0.015 μgm^{-2}s^{-1}), since there is more sea-ice in the region around Utqiaġvik and south west of Alaska in the January simulation (not shown here). Two further simulations are performed to explore model sensitivity to sea-ice fractions. First, ERA5 sea-ice fractions are set equal to zero to the north, west, and east of Utqiaġvik to examine the effect
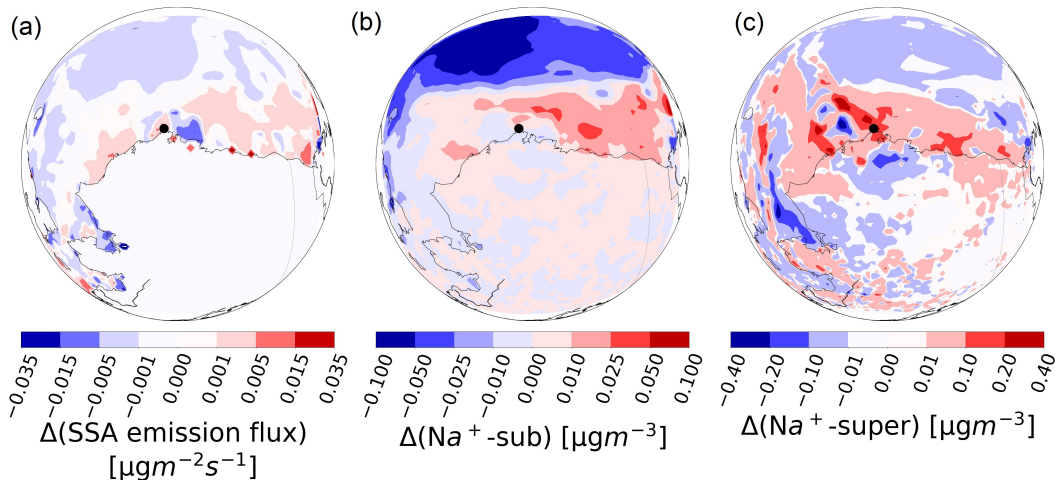
Figure 9. ~~Evaluation~~ Average differences between ALASKA_NEW_FEB and SSA_WS_DEP_FEB showing the effect of ~~modelled aerosol composition against in-situ observations at Utqiaġvik~~ switching from FNL to ERA5 sea-ice fractions during the February campaign for (a) ~~January and~~ SSA emission flux (~~b~~μgm^{-2}s^{-1})~~February 2014 campaign in UTC (00z, 12z~~(b) sub-micron Na$^+$ and ~~STP conditions~~(c) super-micron Na$^+$ mass concentrations in μgm^{-3}. ~~The black lines show model results from~~ All the ~~ALASKA_CONTROL_JAN/FEB; the red lines show the ALASKA_NEW_JAN/FEB, while the daily observations~~ results are shown ~~as blue crosses~~at the surface. ~~The corresponding model daily averages are~~ Utqiaġvik is shown ~~as black diamonds for~~ by the ~~ALASKA_CONTROL_JAN/FEB runs and as red pentagons for ALASKA_NEW_JAN/FEB runs~~black dot. ~~Green circles show observed ss-SO$_4^{2-}$. The grey lines and pentagons show modelled ss-SO$_4^{2-}$ for ALASKA_NEW_JAN/FEB, while dark turquoise pentagons show modelled ss-SO$_4^{2-}$ for ALASKA_CONTROL_JAN/FEB. See~~ Note the ~~text for more details~~different scales.

of having ice-free conditions and the presence of open leads locally (as seen by the radar). Second, ERA5 sea-ice fractions are set equal to 0.75 north, west, east of Utqiaġvik and northwest of Alaska. In both cases, the model is run on a windy day (28 February 2014). The first sensitivity test leads to an increase in SSA emission fluxes by up to 0.2 μgm^{-2}s^{-1} when sea-ice fractions equal zero and to an increase of up to 1.2 μgm^{-3} and 0.05 μgm^{-3} in super-micron and sub-micron Na$^+$, respectively. The second sensitivity test yields similar results. This is because ERA5 sea-ice fractions are higher (more sea-ice) than the test case (0.75) leading to small increases in the SSA emission fluxes especially east of Utqiaġvik. Again, super-micron SSA (increases of up to 1.5 μgm^{-3}) are affected more than sub-micron SSA. These results illustrate the regional sensitivity of super-micron SSA rather than sub-micron SSA to prescribed sea-ice fractions. Missing mechanisms influencing sub-micron SSA emissions may need to be included in the model such as SSA production of, in particular ultrafine particles, from breaking waves in the surf zone *(Clarke et al., 2006)*. However, information about wave-breaking activity in the surf zone during winter along the northern Alaskan coast is needed to address this.
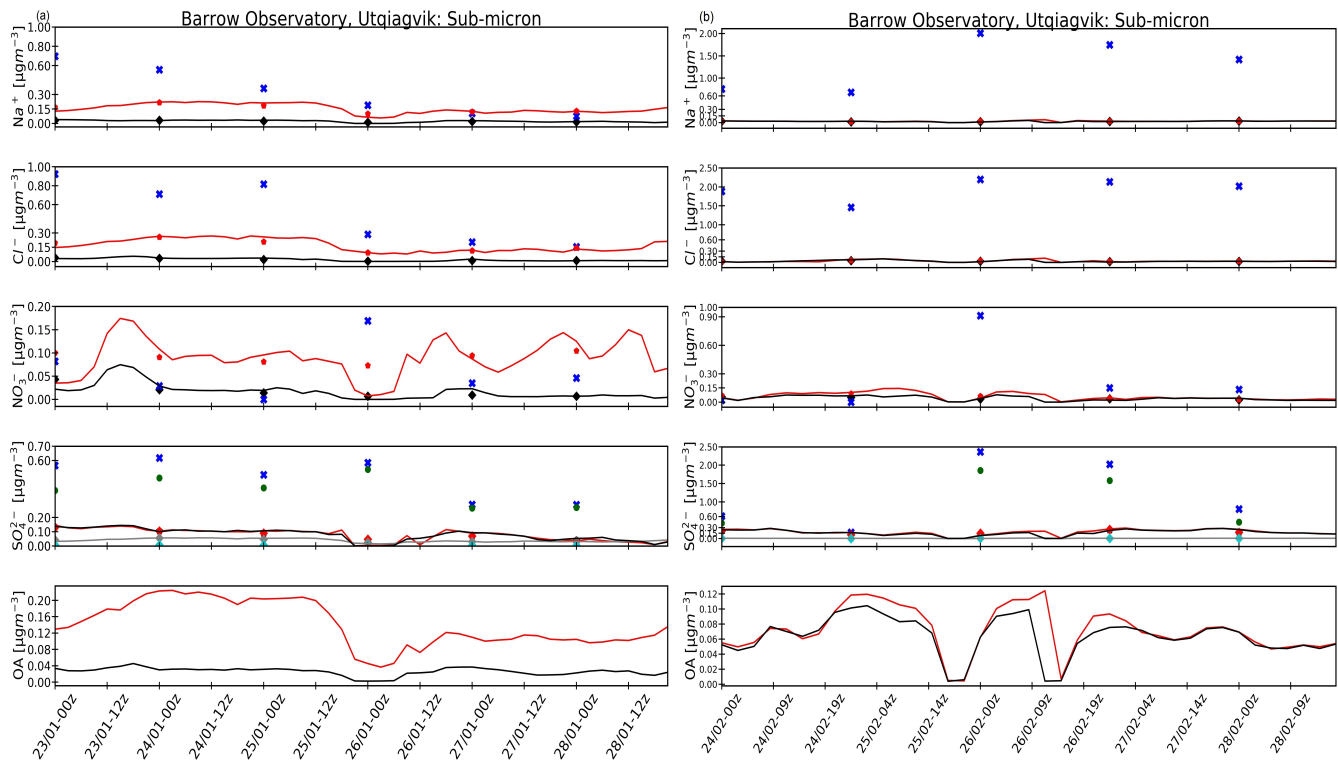
Figure 10. Evaluation of daily averaged modelled aerosol composition against in-situ daily observations at Utqiaġvik during the (a) January and (b) February 2014 campaign in UTC and STP conditions. The black lines show model results from the ALASKA_CONTROL_JAN/FEB; the red lines show the ALASKA_NEW_JAN/FEB, while the daily average observations are shown as blue crosses. The corresponding model daily averages are shown as black diamonds for the ALASKA_CONTROL_JAN/FEB runs and as red pentagons for ALASKA_NEW_JAN/FEB runs. Green circles show observed ss-SO_4^{2-}. The grey lines and pentagons show modelled ss-SO_4^{2-} for ALASKA_NEW_JAN/FEB and dark turquoise pentagons show modelled daily average ss-SO_4^{2-} for ALASKA_CONTROL_JAN/FEB. See the text for more details.

6.4 Evaluation against observations in northern Alaska

Results from runs at 20km with and without the main changes included in the sensitivity tests (local source of marine organics, higher wind speed dependence and ERA-5 sea-ice fractions) are compared to sub-micron aerosol observations at Utqiaġvik for both the January and February 2014 ~~campaign~~ periods (see Fig. 10). We note that there are no super-micron observations ~~during the simulation periods~~ available due to the weekly sampling frequency. It is interesting to compare to these periods since the observations show different behaviours. While observed sub-micron Na$^+$ and Cl$^-$ concentrations reached up to 2.5 μgm^{-3} in February, they did not exceed 1 μgm^{-3} during January. As noted earlier such high concentrations were not observed at Alert and Villum during January and February 2014. The January run, including all the updates (ALASKA_NEW_JAN), captures better sub-micron Na$^+$ and Cl$^-$ (reduced biases and RMSEs - see APPENDIX F, Table F1) although it underestimates observations
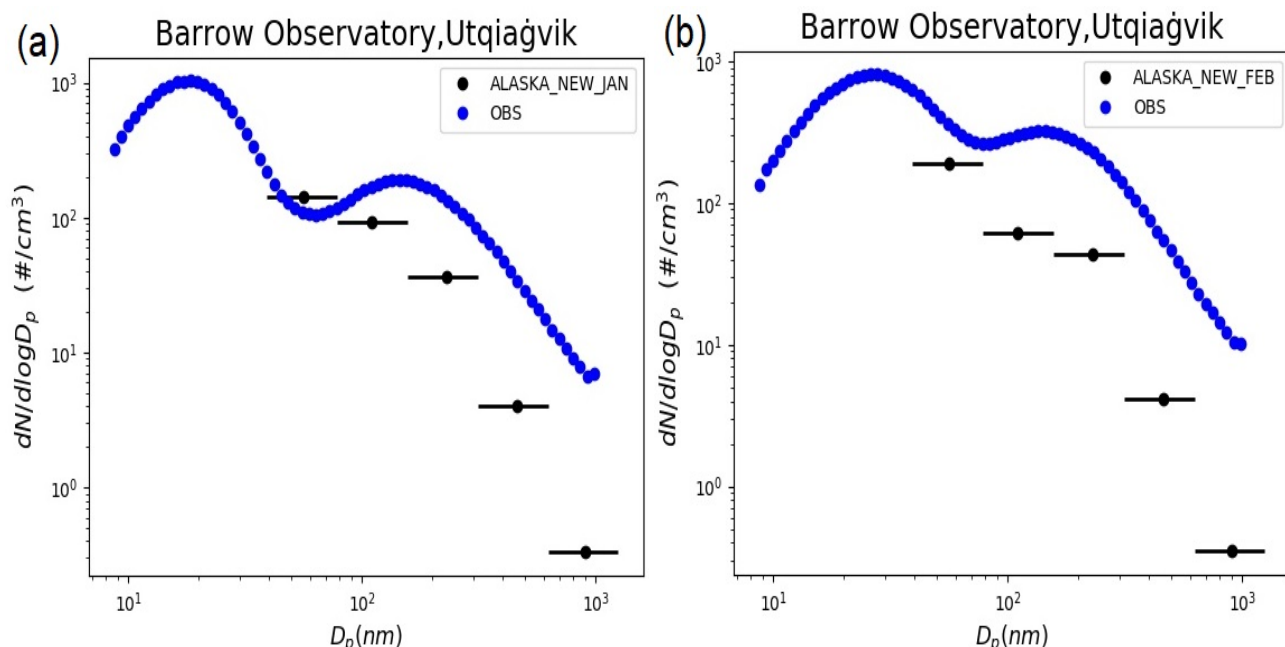
Figure 11. Averaged modelled (black) and measured (blue) ~~particle~~ number size distributions ~~of particles~~ (y-axis), in particle number(#)/cm^{-3}, during (a) January and (b) February 2014 campaign periods at Utqiaġvik as a function of diameter (D$_p$) in nm. The model results are ~~based on~~ from the ALASKA_NEW_JAN and ALASKA_NEW_FEB simulations. The black dot is plotted in the middle of each MOSAIC bin. The line left and right of each dot indicates the minimum and the maximum of range each bin.

by up to 0.6 and 0.8 μgm^{-3} (Fig. 10a), respectively, while sub-micron NO$_3^-$ is slightly overestimated. Biases and RMSEs (see APPENDIX F, Table F2) are also slightly improved for February although sub-micron Na$^+$, Cl$^-$ are still underestimated by up to 1.5 μgm^{-3}. Slightly more NO$_3^-$ is simulated in January, even if the model still underestimates the elevated observations. Up

620 to six times more OA is simulated during both periods in better agreement with reported observations *(Moschos et al., 2022b)*, as discussed in section 5.2. The sensitivity tests discussed in this section do not directly address the model underestimation of elevated episodes of sub-micron total SO$_4^{2-}$, since it is mostly nss-SO$_4^{2-}$, and thus the changes are small (during both simulation periods). We note that these runs at 20km are for periods including elevated aerosols and are thus more challenging for the model to reproduce. Runs at higher resolution may be needed to better resolve, for example, sea-ice distributions.

625 Observations of particle number concentration are also used to validate the regional model results at Utqiaġvik (see Fig. 11). High number concentrations are observed during both periods, up to 10^3 particles per cm^3, especially for particle sizes less than 20 nm. *Freud et al. (2017)* reported similar wintertime magnitudes in the accumulation mode (diameter range 100-150 nm) at Utqiaġvik, averaging between 1 x 10^2 and 2 x 10^2 particles per cm^3, whereas ~~the magnitude is smaller for particles with diameters~~ smaller number concentrations were reported for particles less than 50nm than shown here. These differences can

630 be explained by the fact that the SMPS data used here does not exclude local/regional pollution based on wind speed criteria unlike *Freud et al. (2017)*. Local or regional pollution influenced by Utqiaġvik town or NSA oil fields could lead to new particle

growth events (small particles) in the absence of sunlight, as discussed by *Kolesar et al. (2017)*. ~~They~~ *Freud et al. (2017)* also noted that particle number concentrations are higher at Utqiaġvik and Tiksi (~~in northern Russia~~sites in proximity to local sources) compared to other Arctic sites (Alert, Villum and Zeppelin). The model tends to underestimate observed number concentrations, especially in the 4th (312.5 to 625.0 nm) and 5th (625.0 to 1250 nm) MOSAIC bins, even if the model compares better in January when measured number concentrations are lower. This is consistent with the evaluation of sub-micron SSA and other aerosol components, particularly for episodes when observed aerosols were enhanced (Fig. 10). Note that the model results cannot be compared to measurements smaller than 39 nm because MOSAIC does not represent these aerosols explicitly and nucleation is parameterised. Inclusion of a source function to account for ultrafine SSA emissions, for example, from breaking waves at the surf zone, may lead to improved model results *(Clarke et al., 2006)*.

Overall the results the results presented so far in this Section show that modelled sub-micron SSA (Na^+, Cl^-), and as a consequence NO_3^-, are more sensitive to using a higher wind speed dependence than sea-ice fractions, over northern Alaska, based on estimated biases and RMSEs for each test simulation (not shown here). Sea-ice fractions have a greater effect on super-micron SSA mass concentrations. Modelled sub-micron OA are more sensitive to a higher wind speed dependence and, to a lesser extent, the introduction of an additional source of local marine organics. However, the latter is highly uncertain.

6.5 Are blowing snow and/or frost flowers a source of sub-micron SSA during wintertime at Utqiaġvik?

Lastly, we consider whether enhanced SSA, in particular in the sub-micron size range, at Utqiaġvik could be due to blowing snow or frost flower sources. As noted earlier, KRP19 found no evidence of blowing snow or frost flowers at this site but that SSA originated from open leads during wintertime. Their findings are supported by the earlier laboratory study of *Roscoe et al. (2011)* who reported that frost flowers are not an efficient source of SSA. However, *Shaw et al. (2010)* found that during winter at Utqiaġvik surface frost flowers forming on sea and lake ice are a source of ~~ocean-derived~~ marine-derived OM. Modelling studies including a source of blowing snow and frost flowers suggest that they are contributing to SSA at this time of year at Utqiaġvik, Alert and Zeppelin *(Xu et al., 2013, 2016; Huang and Jaeglé, 2017; Rhodes et al., 2017)*.

~~=1cm Average sub-micron modelled and observed depletion factors, following *Frey et al. (2020)*, during the campaign in January and February 2014 at Utqiaġvik. Model results for ALASKA_NEW_JAN and ALASKA_NEW_FEB simulations are shown here, respectively. Observations refer to sub-micron data from NOAA. Depletion Factors Model Observations $DF_{SO_4^{2-}}$= -0.94 -7.56 DF_{Na^+} -0.95 -0.09 $DF_{SO_4^{2-}}$ -2.2 -2.15 DF_{Na^+} -1.2 -0.19 DF_{Br^-} - 0.063~~

To investigate whether blowing snow or frost flowers could also be a source of SSA during the campaign at Utqiaġvik, depletion factors are estimated following *Frey et al. (2020)* (FR20 from now on). FR20 reported that blowing snow was the main source of SSA rather than frost flowers and open-leads in Antarctic wintertime, based on SO_4^{2-} and bromide (Br^-) depletion in SSA being indicative of a blowing snow origin, and not seawater. Other studies also suggested that blowing snow and frost flowers near Utqiaġvik are characterised by SO_4^{2-} depletion compared to seawater *(Douglas et al., 2012; Jacobi et al., 2012)*.

Here, depletion factors are calculated using modelled and observed sub-micron aerosol mass concentrations during the campaign periods.

=1cm

Table 5. Average sub-micron modelled and observed depletion factors, following *Frey et al. (2020)*, during the campaign periods in January and February 2014 at Utqiaġvik. Model results for ALASKA_NEW_JAN and ALASKA_NEW_FEB simulations are shown, respectively. Observations refer to sub-micron data from NOAA.

Depletion Factors	Model	Observations
January campaign		
$DF_{SO_4^{2-}}$	-0.94	-7.56
DF_{Na^+}	-0.95	-0.09
February campaign		
$DF_{SO_4^{2-}}$	-2.2	-2.15
DF_{Na^+}	-1.2	-0.19
DF_{Br^-}	-	0.063

More specifically, total SO_4^{2-} depletion relative to Na^+ ($DF_{SO_4^{2-}}$), Na^+ depletion relative to Cl^- (DF_{Na^+}) and Br^- depletion relative to Na^+ (DF_{Br^-} only for observations in this case) are calculated using the following equation:

$$DF_x = 1 - \frac{R_{smpl}}{R_{RSW}} \tag{6}$$

where R is the mass ratio (x:y), of species x,y in the model or in the sample (smpl), and in reference seawater (RSW)

670 *(Millero et al., 2008)*. A depletion factor (DF_x) between zero (small) and 1 (strong) indicates 0–100% depletion, whereas DF_x less than zero indicates enrichment. FR20 suggested, based on depletion of SO_4^{2-} relative to Na^+, that most SSA originates from blowing snow on sea-ice with minor contributions from frost flowers, and not from open leads.

The average values of modelled and observed DFs are shown in Table 5. Total SO_4^{2-} is enriched relative to Na^+ in both the observations and the model results during both campaign periods, in contrast to FR20 who reported substantial depletion. In

675 February, observed and model results both indicate SO_4^{2-} enrichment relative to seawater, whereas in January, model results are less ~~enrichment~~ enriched compared to the observations, possibly due to underestimation of nss-SO_4^{2-}. In January, observed total SO_4^{2-} concentrations are 7.56 times higher than in reference seawater, possibly due to internal mixing with anthropogenic nss-SO_4^{2-}, as noted by KRP18. Modelled total SO_4^{2-} is less enriched than the observations (0.94 times higher than in reference seawater), likely due the model underestimation of nss-SO_4^{2-}. FR20 did report a case of enrichment due to possible contami-

680 nation from the ship, an anthropogenic source. The Na^+ depletion factor also shows enrichment during both campaigns, albeit more negligible in the observations than in the model. Observed Na^+ depletion relative to Cl^- is 1.09 or 1.19 times more than in reference seawater, during January and February, respectively. Our analysis suggests that blowing snow and frost flowers are not a significant source of SSA, at least during ~~the campaign .~~ this campaign in winter 2014.

~~=1cm Average modelled and observed molar ratios for sub-micron SSA, following *Kirpes et al. (2019)*, during the campaign~~

685 ~~in January and February 2014 at Utqiaġvik. Model results from ALASKA_NEW_JAN and ALASKA_NEW_FEB simulations~~

SSA can also play an important role in polar tropospheric ~~ozone~~ O_3 and halogen chemistry through the release of active bromine during spring *(Fan and Jacob, 1992; Simpson et al., 2007; Peterson et al., 2017)*. Reactions involving bromine are an important sink of ~~ozone (O_3)~~ O_3 (e.g. *(Barrie, 1986; Marelle et al., 2021)*). Br^- depletion relative to Na^+ is calculated only during February since observed Br^- was zero during the January campaign period. The results for February show a small depletion indicating a seawater origin. The observed mass ratio of Br^- to Na^+ ranges between 0.0057 and 0.0059, while the mass ratio of Br^- to Na^+ in reference seawater is equal to 0.006. FR20 reported no or little Br^- depletion relative to Na^+ due to Br^- losses at the surface and small depletion further aloft (in Antarctica). For a more comprehensive analysis, observations are required at different locations and altitudes across northern Alaska. We note that the version of WRF-Chem used in this study does not include halogen chemistry. It has since been implemented in a later version by *Marelle et al. (2021)* to examine springtime ozone depletion events at Utqiaġvik. Heterogeneous reactions on SSA from the sublimation of lofted blowing snow were also included. Their results suggested that blowing snow could be a source of SSA during spring although it should be noted that this model version, including blowing snow as a source of SSA, overestimated SSA (d_a < 10 μm) at Arctic sites, such as Alert and Villum during spring and did not examine wintertime conditions.

=1cm

Table 6. Average modelled and observed molar ratios for sub-micron SSA, following *Kirpes et al. (2019)*, during the campaign periods in January and February 2014 at Utqiaġvik. Model results from ALASKA_NEW_JAN and ALASKA_NEW_FEB simulations are used. Observations refer to sub-micron data from NOAA.

Molar ratios	Model	Observations
January campaign		
total-SO_4^{2-}:Na^+	0.12	0.55
Cl^-:Na^+	0.71	1.1
February campaign		
total-SO_4^{2-}:Na^+	1.5	0.2
Cl^-:Na^+	0.8	1.08

Finally, modelled and observed molar ratios of sub-micron Cl^-:Na^+ and SO_4^{2-}:Na^+ are estimated to further examine the origins of SSA and compare our findings with KPR19 (see Table 6). The averaged molar ratios of sub-micron Cl^-:Na^+ and SO_4^{2-}:Na^+ derived here for the campaign periods (Table 6) agree with KRP19 (Cl^-:Na^- equal to 1.08, see KRP19 supplement - Table S3, text and references within). They indicate a seawater origin, and confirm the findings of KRP19 that there was no evidence for blowing snow and frost flowers as a source of SSA during the Utqiaġvik campaign, also in agreement with previous studies *(May et al., 2016)*. Model averaged molar ratios are smaller in magnitude than the observations. These discrepancies could be due to the fact that the model underestimates sub-micron SSA and SO_4^{2-}, for the reasons noted earlier. Differences could also be due to issues with modelled SSA lifetime and chemical processing during long-range transport. *May et al. (2016)*

used Cl^-:Na^+ molar ratio enrichment factors as an indicator of long-range transport influence on SSA at Utqiaġvik. They reported that Cl^- depletion was larger for aged sub-micron than for aged super-micron SSA due to a longer lifetime, in line with other studies *(Leck et al., 2002; Hara et al., 2002)*. The regional results (ALASKA_NEW_JAN, ALASKA_NEW_FEB) indicate that modelled sub-micron Cl^- has undergone significant atmospheric processing. Thus, the regional model results, influenced by the simulation at 100km, have too much aged sub-micron SSA, while the contribution from locally produced sub-micron SSA may be too low in the model (modelled enrichment factors equal to 0.5 and 0.4 during January and February simulation periods, respectively, lower than the threshold (0.75) defined by *May et al. (2016)*). On the other hand, modelled enrichment factors for super-micron are equal to 0.6 and 0.85 during January and February, respectively, indicating that there is a possibly background influence on super-micron SSA during January, while they are locally produced during February. KRP18 reported the presence of both fresh (locally-produced) SSA and aged (partially Cl^--depleted) SSA for sub-micron SSA, while super-micron were mostly fresh (KRP18, Figure 2). Based on the analysis above (including observations), there is little evidence suggesting that blowing snow or frost flowers are a significant source of SSA at Utqiaġvik during winter, and open leads are an important primary source, in agreement with KRP19.

6.6 Conclusions

In this study, the ability of the WRF-Chem model to simulate wintertime Arctic aerosols is assessed with a particular focus on SSA under Arctic Haze conditions. The inclusion of updated treatments of SSA emissions leads to improved simulation of SSA over the wider Arctic compared to the still widely used *Gong et al. (1997)*-based source function included in the base model. Na^+ and Cl^- biases are reduced by a factor of 7 to 16 compared to observations at Alert, Villum and Zeppelin, and by a factor of 4 compared to super-micron Na^+ and Cl^- data at Utqiaġvik. The addition of a SST dependence has a larger effect on modelled SSA compared to updating the wind speed dependence, and is responsible for two-thirds of the reductions in super-micron/coarse mode SSA, due to low SSTs in the Arctic. The use of a more realistic lower wind speed dependence, based on satellite data, also results in lower super-micron SSA, but up to 5 times less compared to the SST dependence. In addition to uncertainties in wind speed and SST dependencies influencing production of SSA, other factors such as seawater composition, wave characteristics, fetch and salinity may also be playing a role and should be considered in future versions of WRF-Chem. Other SST dependencies could also be tested which could increase sub-micron SSA at low temperatures *(Sofiev et al., 2011; Salter et al., 2015; Barthel et al., 2019)*. In addition, missing sources of ultrafine SSA particles, for example, due to breaking waves at the coast, could also be included by defining a surf zone in the model *(Clarke et al., 2006)*. In all cases, more field data is needed to understand and develop source functions for SSA specific to the Arctic during winter.

Results from this study also highlight the importance of interactions between SSA and other inorganic aerosols, notably NO_3^-, which have largely anthropogenic origins, and contribute to wintertime Arctic Haze. Improved simulation of Na^+ and Cl^- leads to less coarse mode and more fine mode NO_3^- in the model, in better agreement with the observations. This is due to less formation of NO_3^- via heterogeneous uptake of HNO_3, primarily in the coarse mode, and more NO_3^- in the fine mode, in line with previous mid-latitude studies. As a result, simulated aerosols in the updated model are slightly less acidic in the

Arctic, improving agreement with some Arctic sites, even if the model tends to ~~have~~ simulate aerosols, which are too acidic (at some sites).

745 Marine organic ~~aerosol and sub-micron sea-spray emissions~~ aerosols are also activated in the model since they are an important component of SSA in the Arctic, and globally, and a source of ss-SO_4^{2-} is also added. Simulated OA is improved at the Simeonof sub-Arctic site with reduced biases, by up to a factor of 4, although, in general, OA is underestimated at sites over the wider Arctic. The addition of ss-SO_4^{2-} agrees well with ss-SO_4^{2-} derived from the observations at most Arctic sites and leads to improved modelled total SO_4^{2-}. However, at Zeppelin and Villum, which are dominated by nss-SO_4^{2-}, this

750 additional source results in further overestimation. While super-micron SO_4^{2-}, primarily of sea-salt origin, is captured better at Utqiaġvik on the northern Alaskan coast, sub-micron SO_4^{2-}, which is primarily nss-SO_4^{2-}, is underestimated at this site during episodes with elevated concentrations, and also at ~~Gates of the Arctic~~ GoA further inland. Model discrepancies in OA and nss-SO_4^{2-} may be due to missing local anthropogenic emissions, coupled with missing heterogeneous or dark reactions leading to secondary aerosol formation. In the case of OA, primary marine emissions may also be underestimated. It can be noted that

755 such underestimations are a common feature in other models *(Whaley et al., 2022)*. ~~Uncertainties~~ The above, combined with uncertainties in model transport and wet and dry deposition processes ~~may also be responsible for deficiencies in modelled~~ contribute to model deficiencies in simulating wintertime Arctic aerosols *(Whaley et al., 2022)*.

Model sensitivity to different processes affecting wintertime SSA over northern Alaska is explored further with the aim to understand, in particular, model underestimation of sub-micron SSA at Utqiaġvik during winter 2014 when field data analysis

760 showed that marine emissions from open leads were an important source of SSA, including marine organics (KRP18, KRP19). Based on observed ratios of OC:Na^+ from the KRP19 campaign, a local source of marine organics is included in model runs at 20km over northern Alaska. This results in higher modelled OA, in better agreement with previous measurements at this site, and other sites such as Alert, although the model still tends to underestimate reported data.

The sensitivity of modelled SSA over northern Alaska to using a higher wind speed dependence, based on Arctic data, is also

765 investigated. This leads to an increase in modelled sub-micron SSA, with the model performing better during January than in February. Model sensitivity to prescribed sea-ice fractions is also explored. In a run with ERA5 instead of FNL sea-ice fractions, modelled super-micron SSA are more sensitive to sea-ice treatments than sub-micron SSA. In general, modelled sub-micron SSA are more sensitive to the use of a higher wind speed dependence rather than the distribution of sea-ice. To improve model simulations in this region, field campaigns are needed to study processes influencing wintertime ~~SSA production~~ production

770 of SSA and to determine more realistic sea-ice fractions which vary on at least a daily basis. The use of satellite sea-ice data, combined with higher resolution simulations over Utqiaġvik, will also help to gain further insights into the influence of open leads on ~~SSA production~~ production of SSA, including marine organics, during wintertime.

Missing local anthropogenic sources could also explain some of the discrepancies in modelled sub-micron SSA. For example, anthropogenic sources of Cl^- may need to be considered, such as coal combustion, waste incineration, and other industrial

775 activities *(Wang et al., 2019)* which are not included in current emission inventories. WRF-Chem, and models in general, also lack anthropogenic emissions of Na^+, which could possibly account for up to 30% of Na^+, as noted by *Barrie and Barrie (1990)*. However, the analysis of depletion factors and molar ratios, presented here for Utqiaġvik, shows that the main source

of fresh SSA is from marine sources including open ocean or leads. We also find no evidence for frost flowers or blowing snow as a source of SSA at Utqiaġvik, in agreement with the findings of KRP19 and previous studies *(May et al., 2016)*. Further insights into wintertime marine SSA sources, including organics are needed, as well as improved quantification of local anthropogenic emissions.

Overall, we find that wintertime SSA at remote Arctic sites contribute between 54% and 84% to total inorganic SSA (observations and improved model results), in agreement with previous findings, that SSA are important contributors to super-micron (coarse mode, TSP) mass concentrations. Ice fractures and the area of open ocean are likely to become more important with decreasing sea-ice cover in the Arctic as a result of climate warming. This may lead to more SSA which can act as CCN or INPs with implications for Arctic aerosol-cloud indirect ~~effects~~feedbacks, notably long-wave radiative ~~forcing which dominates~~ effects which dominate in winter *(Eidhammer et al., 2010; Partanen et al., 2014)*. As well as ground-based measurements, vertical profiles of SSA components are also needed to better understand SSA sources and their impacts on clouds. Such studies will ultimately help to reduce uncertainties in estimates of aerosol-cloud indirect radiative effects and the magnitude of the associated radiative cooling *(Horowitz et al., 2020)* or warming *(Zhao and Garrett, 2015)*.

Code availability. The code used to calculate SSA emissions in this study is available on Zenodo as: Ioannidis et al.(2023) https://doi.org/10.5281/zenodo.7502210

Data availability. ECLIPSE v6b emissions are available online at https://previous.iiasa.ac.at/web/home/research/researchPrograms/air/ECLIPSEv6b. html. All data used in the present paper for Zeppelin and Alert are open access and are available at the EBAS database infrastructure at NILU - Norwegian Institute for Air research: http://ebas.nilu.no/. Observations for Villum are obtained after personal communication with Henrik Skov. Observations from IMPROVE database can be obtained from: http://views.cira.colostate.edu/fed/QueryWizard/. Sub- and super-micron aerosol mass concentrations at Utqiaġvik, Alaska can be obtained from the follow link: https://saga.pmel.noaa.gov/data/stations/. The SMPS data are obtained from ftp://ftp.cmdl.noaa.gov/aerosol/brw/smps/. High spatial resolution images of sea-ice cover are obtained from (http://seaice.alaska.edu/gi/data/barrow_radar). Meteorological data used in this study at Utqiaġvik are from National Oceanic and Atmospheric Administration / Earth System Research Laboratory / Global Monitoring Division (NOAA/ESRL/GMD) Baseline Observatories (https://esrl.noaa.gov/). Also radiosonde data (every 12h) are derived from Integrated Global Radiosonde Archive version 2 (IGRA 2) *(Durre et al. (2018))*.

Table A1. WRF-Chem Land ~~Surface model's~~ surface (NOAH MP) ~~parametrization~~parametrisation scheme. "Opt_" indicates the namelist option for NOAH MP.

NOAH MP Parametrization	
Dynamic Vegetation (DVEG)	On
Stomatal Resistance	Ball-Berry *Ball et al. (1987),*
	Collatz et al. (1991),
	Collatz et al. (1992), Bonan (1996), Sellers et al. (1996)
Surface layer drag coefficient (opt_sfc)	Original ~~Noah~~ NOAH *Chen et al. (1997)*
Soil moisture for stomatal resistance (opt_btr)	~~Noah~~ NOAH (soil moisture)
Runoff (opt_run)	TOPMODEL with groundwater *Niu et al. (2007)*
Supercooled liquid water (opt_frz)	no iteration *Niu and Yang (2004)*
Soil permeability (opt_inf)	linear effects, more permeable ~~yue Niu and liang Yang (2006)~~*(Niu and Yang, 2006)*
Radiative transfer (opt_rad)	modified two-stream
	(gap = F(solar angle, 3D structure ...)<1-FVEG)
	Yang and Friedl (2003), Niu and Yang (2004)
Ground surface albedo (opt_alb)	BATS *Yang Z.-L. and Vinnikov. (1997)*
Precipitation (snow/rain) partitioning (opt_snf)	*Jordan (1991)*
Soil temperature lower boundary (opt_tbot)	TBOT at ZBOT (8m) read from a file (original ~~Noah~~NOAH)
Soil/snow temperature time scheme (opt_sfc)	semi-implicit; flux top boundary condition
Surface resistance to evaporation/sublimation (opt_rsf)	*Sakaguchi and Zeng (2009)*
Glacier treatment (opt_gla)	include phase change of ice

Appendix A

Following *Monaghan et al. (2018)*, NOAH-MP parameter file MPTABLE.TBL has been modified, and it can be used for
805   simulations over Alaska. These modifications improved the model's capability to capture cold surface temperature and meteorological profiles (e.g. wind speed, relative humidity, temperature) over Alaska.

Appendix B

Fuentes size-resolved sea-spray source flux $(dF_0/dlogD_{p0})$ in $m^{-2}s^{-1}$:

$$\frac{dF_0}{dlogD_{p0}} = \frac{dF_p}{dlogD_{p0}} \times W(U) = \frac{Q}{A_b} \times \frac{dN_T}{dlogD_{p0}} \times W(U) \tag{B1}$$

where $W(U)$ is Monahan and O'Muircheartaigh whitecap coverage, $dF_p/dlogD_{p0}$ is the size-resolved particle flux (F_p) per unit time and water surface covered by bubbles, D_{p0} (in nm) is the dry diameter, Q is the sweep air flow, A_b is the total surface area covered by bubbles, $dN_T/dlogD_{p0}$ is the sub-micron particle size distribution (the sum of four log-normal modes) and is equal to:

$$\frac{dN_T}{dlogD_{p0}} = \sum_{i=1}^{4} \frac{dN_{T,i}}{dlogD_{p0}} = \sum_{i=1}^{4} \frac{N_{T,i}}{\sqrt{2\pi}\times log\sigma_i} \times exp\left[-\frac{1}{2}\times\left(\frac{log\frac{D_{p0}}{D_{p0g,i}}}{log\sigma_i}\right)^2\right] \tag{B2}$$

where i is the sub-index for the mode number and N_i, $D_{p0g,i}$ and σ_i are the total particle number, geometric mean and geometric standard deviation for each log-normal mode g. $N_{T,i}$ and $D_{p0g,i}$ depend on parameters a_i and β_i derived from polynomial and exponential regressions defining the total particle number and geometric mean diameter of the log-normal modes and can be found in Table 5 in *Fuentes et al. (2010)*.

Table C1. ~~RMSes~~Root-mean-square errors (RMSEs), in μgm^{-3}, averaged over January and February 2014 for CONTROL and HEM_NEW simulations compared to the observations. NA stands for ~~Not~~ not available.

	CONTROL	HEM_NEW	CONTROL	HEM_NEW	CONTROL	HEM_NEW	CONTROL	HEM_NEW	CONTROL	HEM_NEW	CONTROL	HEM_NEW
	Na^+		Cl^-		NO_3^-		nss-SO_4^{2-}	nss-SO_4^{2-}/ ss-SO_4^{2-}	NH_4^+		OA	
Alert	0.91	0.18	1.2	0.19	0.3	0.19	0.1	0.09/ 0.03	0.011	0.01	NA	NA
Villum	1.4	0.3	2.1	0.3	0.26	0.15	0.1	0.06/ 0.07	0.01	0.01	NA	NA
Zeppelin	4.4	0.3	6.5	0.3	0.4	0.3	0.3	0.3/ 0.2	0.08	0.07	NA	NA
Utqiagvik super-micron	0.37	0.25	0.48	0.51	0.3	0.17	0.05	0.06/ 0	0.004	0.004	NA	NA
Utqiaġvik sub-micron	0.66	0.67	0.361	0.364	0.162	0.158	0.88	0.73/ 0.18	0.11	0.09	NA	NA
GoA	0.9	0.3	1.2	0.3	0.3	0.3	0.2	0.16/ 0.08	NA	NA	0.28	0.27
Simeonof	2.5	0.6	3.7	0.7	0.23	0.2	0.25	0.25/ 0.19	NA	NA	0.1	0.08

Appendix C

820 ~~In this APPENDIX, the~~ The RMSEs are shown for each site and aerosol component at 100km.

Table D1. Estimated mean neutralized factor, f, using the observations and the results from the two quasi-hemispheric simulations (100km), CONTROL and HEM_NEW at the different sites. f is not estimated for Simeonof and GoA sites as there are ~~not~~ no observations of NH_4^+.

	Observations	CONTROL	HEM_NEW
Alert	0.26	0.14	0.26
Villum	0.46	0.12	0.26
Zeppelin	0.19	0.12	0.11
Utqiaġvik super-micron	0.18	0.01	0.08
Utqiaġvik sub-micron	0.4	0.6	0.7

Appendix D

To investigate aerosol acidity, the mean neutralized factor (f) is calculated as the ratio of NH_4^+ to the sum of ($2nss$-SO_4^{2-} + NO_3^-), in molar concentrations, following *Fisher et al. (2011)*, for sites in the Arctic with available observations of these aerosols. When f is equal to 1 then aerosols are assumed to be neutralized, while when f < 1 then aerosols are acidic, and

825 more acidic when f is closer to zero *(Fisher et al., 2011)*. In general, higher molar concentrations were observed for nss-SO_4^{2-} compared to NO_3^- and NH_4^+. Table D1 shows f for observations and the two 100km simulations at the different sites. Overall, modelled f increases due to the improved treatment of SSA and the associated influence on NO_3^- via heterogeneous reactions. Since aerosols are assumed to be internally mixed in the model, NH_4^+ and nss-SO_4^{2-} mass concentrations also vary between the two simulations. Thus, aerosols in HEM_NEW tend to be less acidic (e.g. at Alert and Villum), due to NO_3^- decreases

830 in the coarse-mode/TSP size range. This leads to better agreement with the observed f at Alert, in particular. At Villum, observed aerosols are less acidic than in the model. This could be due to the fact that the model has more NH_4^+ compared to the observations. Only small changes are found at Utqiaġvik between the two runs, and the model tends to have aerosols which are slightly more acidic (super-micron) and less acidic (sub-micron) compared to the observations. The small increase in model sub-micron f at Utqiaġvik could be due to the increase in sub-micron NO_3^- and insignificant changes in NH_4^+ and

835 nss-SO_4^{2-}. Differences with the observed values could be explained by underestimation of nss-SO_4^{2-} at this site. The calculated f for observations could also be biased low (too acidic), since some of the NO_3^- and SO_4^{2-} are present as Na_2SO_4 and $NaNO_3$ in the atmosphere, which are not measured.

Appendix E

Surface observations are used to validate the meteorological conditions that occur at Utqiaġvik. The model is validated against

840 the surface (hourly) observations obtained from ~~National Oceanic and Atmospheric Administration / Earth System Research Laboratory / Global Monitoring Division (NOAA/ESRL/GMD) Baseline Observatories~~NOAA. Also, radiosondes data are used
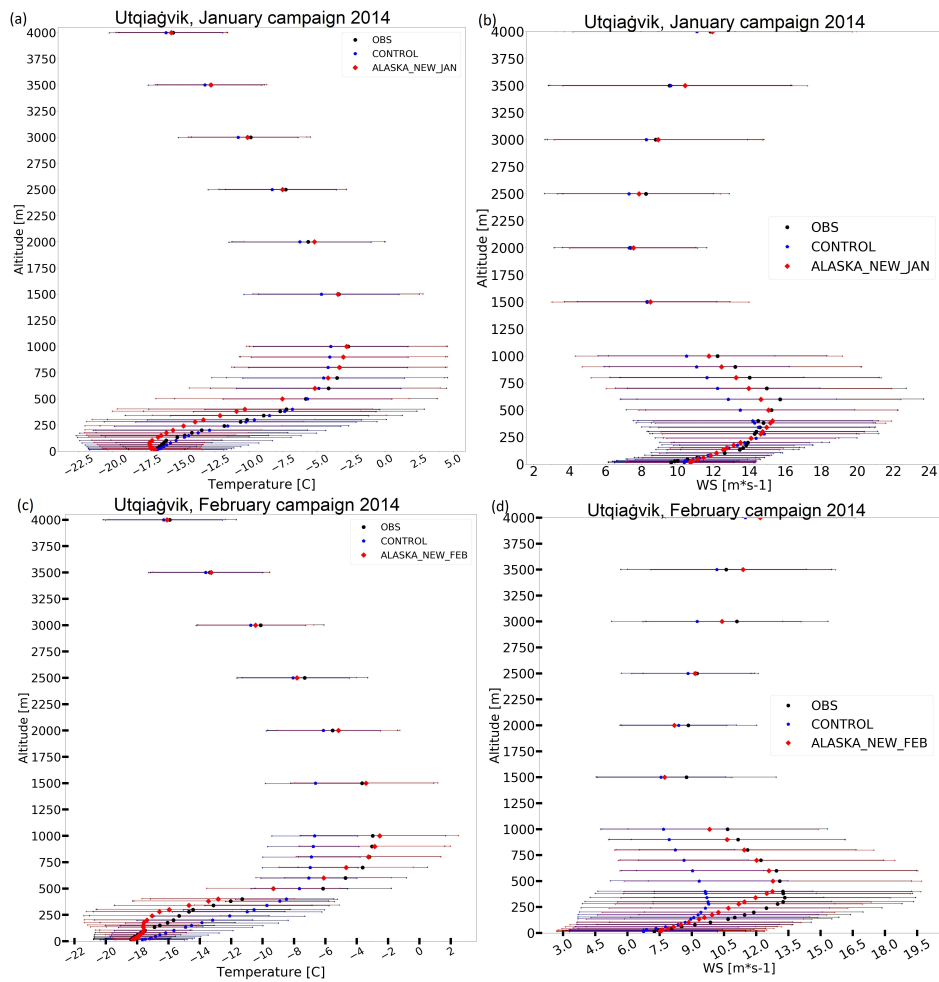
Figure E1. Average temperatures, in degrees C, and wind speeds, in ms⁻¹, as a function of altitude (m), up to 4km, during (a,b) January and (c,d) February campaign in 2014, at Utqiaġvik, Alaska. The observations are shown in black (circle)circles. The blue pentagon shows pentagons show the model results for the CONTROL simulation (at 100km) and the red diamond shows diamonds show the model results for the NEW_ALASKA_JAN and NEW_ALASKA_FEBsimulation. Observations are derived from IGRA2 and are available every 12h (0Z and 12Z, UTC). For the comparison, model output at 0 and 12Z UTC are used. The corresponding horizontal lines show the standard deviation.

to evaluate the model's performance at different altitudes. Radiosonde data (every 12h) are derived from Integrated Global Radiosonde Archive version 2 (IGRA 2) (*Durre et al. (2018)*). Site Utqiaġvik site is located at latitude: 71.2N and longitude: -156.7. In the future, more detailed studies it is advisable to investigate the meteorological and synoptic conditions that occur at each site within Arctic. A detailed focus on the meteorology and removal treatments at lower latitudes to minimize potential uncertainties linked to transport errors in the model is also desirable. W.
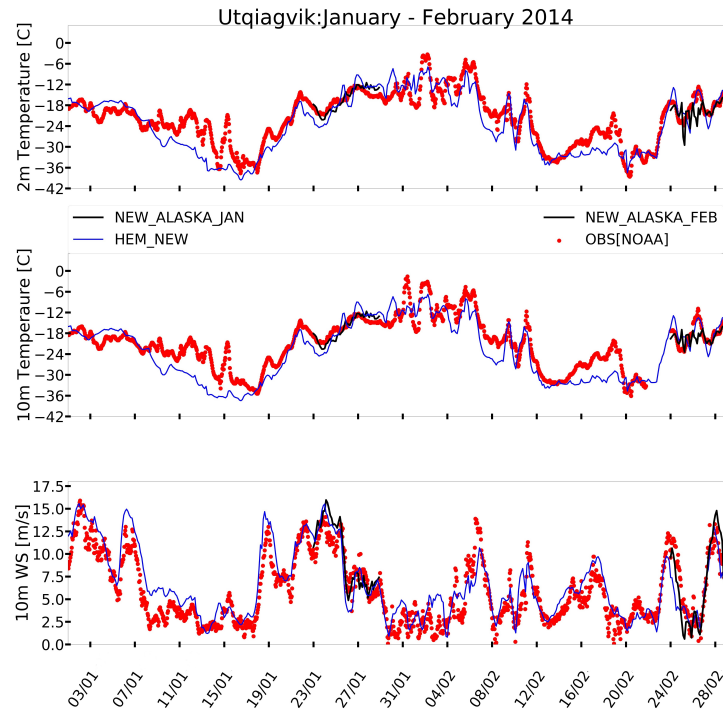
Figure E2. Time series of observed and modelled 2m and 10m ~~temperature~~temperatures, and 10m wind ~~speed~~speeds, at ~~Barrow~~Utqiaġvik, Alaska, in UTC. The observations are shown in red ~~and derived~~ are from the NOAA ~~observatory~~Observatory. The blue line shows the results for the HEM_NEW simulation at 100km, while the black ~~line shows the~~ lines show results for ALASKA_NEW_JAN and ALASKA_NEW_FEB simulations at 20km. The observations are hourly, while the model output is every 3h.

Table E1. Biases and RMSEs, in temperature (^{o}C), wind speed (ms^{-1}) and wind directions (degrees), are calculated between ALASKA_NEW_JAN, ALASKA_NEW_FEB and in-situ meteorological ~~parameters derived~~ observations from the NOAA ~~Baseline Observatories~~ Observatory during the campaign ~~'s~~ periods in January and February 2014. ~~Bias was~~ Absolute biases are calculated as the difference between model ~~simulation~~ simulations and the observations.

	January 2014		February 2014	
	Bias	RMSE	Bias	RMSE
2m Temperature	0.1	1.9	-1.0	3.2
10m Temperature	-0.03	1.8	-0.66	2.7
10m Wind speed	0.08	1,4	-0.33	1.7
10m Wind direction	-11.2	13.2	-11.2	39.0

Table F1. ~~Biases~~ Absolute biases and RMSEs, in aerosol mass concentrations (in μgm^{-3}, ~~are calculated for aerosols~~) at Utqiaġvik, north of Alaska, during January 2014 ~~and~~ for ALASKA_CONTROL_JAN and ALASKA_NEW_JAN simulations at 20km, compared to observations.

	ALASKA_CONTROL_JAN		ALASKA_NEW_JAN	
	Bias	**RMSE**	**Bias**	**RMSE**
Na$^+$	-0.31	0.38	-0.22	0.27
Cl$^-$	-0.50	0.58	-0.35	0.44
NO$_3^-$	-0.040	0.07	0.039	0.06
SO$_4^{2-}$	-0.4	0.41	-0.39	0.41

Table F2. ~~Biases~~ Absolute biases and RMSEs, in aerosol mass concentrations (in μgm^{-3}, ~~calculated for aerosols~~) at Utqiaġvik, north of Alaska, during February 2014 ~~and~~ for ALASKA_CONTROL_FEB and ALASKA_NEW_FEB simulations at 20km, compared to observations.

	ALASKA_CONTROL_FEB		ALASKA_NEW_FEB	
	Bias	**RMSE**	**Bias**	**RMSE**
Na$^+$	-1.30	1.40	-1.29	1.39
Cl$^-$	-1.91	1.92	-1.90	1.90
NO$_3^-$	-0.20	0.40	-0.18	0.38
SO$_4^{2-}$	-1.03	1.33	-1.01	1.31

Appendix F

~~Here the bias and RMSE are shown~~ Biases and RMSEs are given calculated between ALASKA_NEW_JAN and ALASKA_NEW_FEB and the observations for Utqiaġvik at 20km. See main text for details.

Author contributions. The first author (EI) implemented the updates, performed the simulations and the analysis, and drafted the paper. KSL designed the study, contributed to the interpretation of results and the analysis, and to writing the paper. JCR, LM and TO contributed to discussions about the model setup, simulations. JCR, LM, KP, RMK, PKQ and LU contributed to the analysis and interpretation of the results. AM and HS contributed to the interpretation of the results. TT and AW contributed to the interpretation of SMPS analysis. All co-authors contributed to the paper and the discussions about the results, as well as for the revision of the manuscript and have approved the final version.

Competing interests. The authors declare that they have no conflict of interest.

Acknowledgements. ~~This study is~~ EI was supported by the PhD programme of the Make ~~our planet great again~~ Our Planet Great Again (MOGPA) French initiative. We also acknowledge support from ~~French ANR~~ the French Agence National de Recherche (ANR) CASPA (Climate-relevant Aerosols and Sources in the Arctic) ~~.~~ project (ANR-21-CE01-0017). French authors also acknowledge support from the French space agency CNES, MERLIN project. Computer modeling performed by ~~Eleftherios Ioannidis~~EI, benefited from access to IDRIS HPC resources (GENCI allocations A009017141 and A011017141) and the IPSL mesoscale computing center (CICLAD: Calcul Intensif pour le Climat, l'Atmosphère et la Dynamique). We acknowledge the use of MOZART-4 global model output available at http://www.acom.ucar.edu/wrf-chem/mozart.shtml. We acknowledge use of the WRF-Chem preprocessor tool mozbc provided by the Atmospheric Chemistry Observations and Modeling Lab (ACOM) of NCAR. We would like to thank Arctic Monitoring and Assessment Programme (AMAP) and Zbigniew Klimont for ECLIPSE v6b anthropogenic emissions. ~~ECLIPSE v6b emissions are available online at .~~ We would like to acknowledge European Commission 7th Framework funded projects: (i) ECLIPSE (Evaluating the Climate and Air Quality Impacts of Short-Lived Pollutants) Project no. 282688, (ii) PEGASOS (Pan-European Gas-Aerosols-Climate Interaction Study) Project no. 265148, (iii) Assessment of hemispheric air pollution on EU air policy' contract no. 07.0307/2011/605671/SER/C3. K.A.P. acknowledges funding from the US National Science Foundation (OPP-1724585). This is PMEL contribution number 5366. L.M.U. acknowledges the Cooperative Institute for Climate, Ocean, and Ecosystem Studies (CIOCES) under NOAA Cooperative Agreement NA20OAR4320271, Contribution No. 2022-1224. Louis Marelle is supported by the European Union's Horizon 2020 research and innovation programme under grant agreement No 101003826, project CRIceS. Also, we would like to thank the IMPROVE database for the aerosol observations in Alaska. IMPROVE is a collaborative association of state, tribal, and federal agencies, and international partners. US Environmental Protection Agency is the primary funding source, with contracting and research support from the National Park Service. The Air Quality Group at the University of California, Davis is the central analytical laboratory, with ion analysis provided by Research Triangle Institute, and carbon analysis provided by Desert Research Institute. ~~Meteorological data provided by NOAA Global Monitoring Laboratory, Boulder, Colorado, USA ().~~ We would like to thank Josh Jones for providing us with detailed maps of sea-ice fraction plots from the radar at Utqiaġvik. The Villum Foundation is gratefully acknowledged for financing the establishment of the Villum Research Station. ~~Finally, we would like to~~ We also thank Aas Wenche (Norwegian Institute for Air Research) and Sharma Sangeeta (Environment and Climate Change Canada, Science and Technology Branch, Toronto, Canada) for providing us with EBAS observations at Zeppelin and Alert, respectively. ~~Authors also want to~~ We thank Canadian Forces Services, Alert, NU for maintaining the site. The observations at Zeppelin have been supported by the Norwegian Environment Agency (grant no. 17078061).

References

Aas, W., Eckhardt, S., Fiebig, M., Platt, S. M., Solberg, S., Yttri, K. E., and Zwaaftink, C. G.: Monitoring of long-range transported air pollutants in Norway. Annual Report 2020., NILU rapport, 2021.

885 Adachi, K., Tobo, Y., Koike, M., Freitas, G., Zieger, P., and Krejci, R.: Composition and mixing state of Arctic aerosol and cloud residual particles from long-term single-particle observations at Zeppelin Observatory, Svalbard, Atmospheric Chemistry and Physics, 22, 14 421–14 439, 2022.

Alexander, B., Park, R. J., Jacob, D. J., Li, Q., Yantosca, R. M., Savarino, J., Lee, C., and Thiemens, M.: Sulfate formation in sea-salt aerosols: Constraints from oxygen isotopes, Journal of Geophysical Research: Atmospheres, 110, 2005.

890 Allan, R. P.: Climate Change 2021: The Physical Science Basis: Working Group I Contribution to the Sixth Assessment Report of the Intergovernmental Panel on Climate Change, WMO, IPCC Secretariat, 2021.

AMAP: AMAP Assessment 2015: Black carbon and ozone as Arctic climate forcers, 2015.

Archer-Nicholls, S., Lowe, D., Utembe, S., Allan, J., Zaveri, R. A., Fast, J. D., Hodnebrog, Ø., Denier van der Gon, H., and McFiggans, G.: Gaseous chemistry and aerosol mechanism developments for version 3.5.1 of the online regional model, WRF-Chem, Geoscientific

895 Model Development, 7, 2557–2579, https://doi.org/10.5194/gmd-7-2557-2014, 2014.

Ball, J. T., Woodrow, I. E., and Berry, J. A.: A model predicting stomatal conductance and its contribution to the control of photosynthesis under different environmental conditions, in: Progress in photosynthesis research, pp. 221–224, Springer, 1987.

Barrie, L. and Barrie, M.: Chemical components of lower tropospheric aerosols in the high Arctic: Six years of observations, Journal of Atmospheric Chemistry, 11, 211–226, 1990.

900 Barrie, L., Staebler, R., Toom, D., Georgi, B., Den Hartog, G., Landsberger, S., and Wu, D.: Arctic aerosol size-segregated chemical observations in relation to ozone depletion during Polar Sunrise Experiment 1992., Journal of Geophysical Research: Atmospheres, 99, 25 439–25 451, 1994.

Barrie, L. A.: Arctic air pollution: An overview of current knowledge, Atmospheric Environment (1967), 20, 643–663, 1986.

Barthel, S., Tegen, I., and Wolke, R.: Do new sea spray aerosol source functions improve the results of a regional aerosol model?, Atmospheric

905 Environment, 198, 265–278, 2019.

Berg, L. K., Gustafson, W. I., Kassianov, E. I., and Deng, L.: Evaluation of a modified scheme for shallow convection: Implementation of CuP and case studies, Monthly weather review, 141, 134–147, 2013.

Berg, L. K., Shrivastava, M., Easter, R. C., Fast, J. D., Chapman, E. G., Liu, Y., and Ferrare, R.: A new WRF-Chem treatment for studying regional-scale impacts of cloud processes on aerosol and trace gases in parameterized cumuli, Geoscientific Model Development, 8,

910 409–429, 2015.

Bonan, G. B.: Land surface model (LSM version 1.0) for ecological, hydrological, and atmospheric studies: Technical description and users guide. Technical note, Tech. rep., National Center for Atmospheric Research, Boulder, CO (United States . . . , 1996.

Bowen, H. J. M. et al.: Environmental chemistry of the elements., Academic Press., 1979.

Browse, J., Carslaw, K., Mann, G., Birch, C., Arnold, S., and Leck, C.: The complex response of Arctic aerosol to sea-ice retreat, Atmos.

915 Chem. Phys, 14, 7543–7557, 2014.

Burrows, S. M., Hoose, C., Pöschl, U., and Lawrence, M. G.: Ice nuclei in marine air: biogenic particles or dust?, Atmospheric Chemistry and Physics, 13, 245–267, 2013.

Calhoun, J. A., Bates, T. S., and Charlson, R. J.: Sulfur isotope measurements of submicrometer sulfate aerosol particles over the Pacific Ocean, Geophysical Research Letters, 18, 1877–1880, 1991.

920 Callaghan, A., de Leeuw, G., Cohen, L., and O'Dowd, C. D.: Relationship of oceanic whitecap coverage to wind speed and wind history, Geophysical Research Letters, 35, 2008.

Callaghan, A. H., Deane, G. B., Stokes, M. D., and Ward, B.: Observed variation in the decay time of oceanic whitecap foam, Journal of Geophysical Research: Oceans, 117, 2012.

Callaghan, A. H., Stokes, M., and Deane, G.: The effect of water temperature on air entrainment, bubble plumes, and surface foam in a

925 laboratory breaking-wave analog, Journal of Geophysical Research: Oceans, 119, 7463–7482, 2014.

Campbell, J. R., Battaglia Jr, M., Dingilian, K., Cesler-Maloney, M., St Clair, J. M., Hanisco, T. F., Robinson, E., DeCarlo, P., Simpson, W., Nenes, A., et al.: Source and Chemistry of Hydroxymethanesulfonate (HMS) in Fairbanks, Alaska, Environmental Science & Technology, 2022.

Carter, W. P.: Documentation of the SAPRC-99 chemical mechanism for VOC reactivity assessment, Contract, 92, 95–308, 2000.

930 Chapman, E. G., Gustafson Jr, W., Easter, R. C., Barnard, J. C., Ghan, S. J., Pekour, M. S., and Fast, J. D.: Coupling aerosol-cloud-radiative processes in the WRF-Chem model: Investigating the radiative impact of elevated point sources, Atmospheric Chemistry and Physics, 9, 945–964, 2009.

Chen, F., Janjić, Z., and Mitchell, K.: Impact of atmospheric surface-layer parameterizations in the new land-surface scheme of the NCEP mesoscale Eta model, Boundary-Layer Meteorology, 85, 391–421, 1997.

935 Chen, Y., Cheng, Y., Ma, N., Wolke, R., Nordmann, S., Schüttauf, S., Ran, L., Wehner, B., Birmili, W., Gon, H. A., et al.: Sea salt emission, transport and influence on size-segregated nitrate simulation: a case study in northwestern Europe by WRF-Chem, Atmospheric Chemistry and Physics, 16, 12 081–12 097, 2016.

Chen, Y., Cheng, Y., Ma, N., Wei, C., Ran, L., Wolke, R., Größ, J., Wang, Q., Pozzer, A., Denier van der Gon, H. A., et al.: Natural sea-salt emissions moderate the climate forcing of anthropogenic nitrate, Atmospheric Chemistry and Physics, 20, 771–786, 2020.

940 Chi, J., Li, W., Zhang, D., Zhang, J., Lin, Y., Shen, X., Sun, J., Chen, J., Zhang, X., Zhang, Y., et al.: Sea salt aerosols as a reactive surface for inorganic and organic acidic gases in the Arctic troposphere, Atmospheric Chemistry and Physics, 15, 11 341–11 353, 2015.

Clarke, A. D., Owens, S. R., and Zhou, J.: An ultrafine sea-salt flux from breaking waves: Implications for cloud condensation nuclei in the remote marine atmosphere, Journal of Geophysical Research: Atmospheres, 111, 2006.

Collatz, G. J., Ball, J. T., Grivet, C., and Berry, J. A.: Physiological and environmental regulation of stomatal conductance, photosynthesis

945 and transpiration: a model that includes a laminar boundary layer, Agricultural and Forest meteorology, 54, 107–136, 1991.

Collatz, G. J., Ribas-Carbo, M., and Berry, J.: Coupled photosynthesis-stomatal conductance model for leaves of C4 plants, Functional Plant Biology, 19, 519–538, 1992.

Cravigan, L. T., Ristovski, Z., Modini, R. L., Keywood, M. D., and Gras, J. L.: Observation of sea-salt fraction in sub-100 nm diameter particles at Cape Grim, Journal of Geophysical Research: Atmospheres, 120, 1848–1864, 2015.

950 De Leeuw, G., Andreas, E. L., Anguelova, M. D., Fairall, C., Lewis, E. R., O'Dowd, C., Schulz, M., and Schwartz, S. E.: Production flux of sea spray aerosol, Reviews of Geophysics, 49, 2011.

Douglas, T. A., Domine, F., Barret, M., Anastasio, C., Beine, H. J., Bottenheim, J., Grannas, A., Houdier, S., Netcheva, S., Rowland, G., et al.: Frost flowers growing in the Arctic ocean-atmosphere–sea ice–snow interface: 1. Chemical composition, Journal of Geophysical Research: Atmospheres, 117, 2012.

955 Druckenmiller, M. L., Eicken, H., Johnson, M. A., Pringle, D. J., and Williams, C. C.: Toward an integrated coastal sea-ice observatory: System components and a case study at Barrow, Alaska, Cold Regions Science and Technology, 56, 61–72, 2009.

Durre, I., Yin, X., Vose, R. S., Applequist, S., and Arnfield, J.: Enhancing the data coverage in the Integrated Global Radiosonde Archive, Journal of Atmospheric and Oceanic Technology, 35, 1753–1770, 2018.

Easter, R. C., Ghan, S. J., Zhang, Y., Saylor, R. D., Chapman, E. G., Laulainen, N. S., Abdul-Razzak, H., Leung, L. R., Bian, X., and Zaveri,
960 R. A.: MIRAGE: Model description and evaluation of aerosols and trace gases, Journal of Geophysical Research: Atmospheres, 109, 2004.

Eckhardt, S., Quennehen, B., Oliviè, D. J. L., Berntsen, T. K., Cherian, R., Christensen, J., Collins, W., Crepinsek, S., Daskalakis, N., Flanner, M., et al.: Current model capabilities for simulating black carbon and sulfate concentrations in the Arctic atmosphere: a multi-model evaluation using a comprehensive measurement data set, Atmospheric Chemistry and Physics, 15, 9413–9433, 2015.

965 Eicken, H., Jones, J., Meyer, F., Mahoney, A., Druckenmiller, M. L., Rohith, M., and Kambhamettu, C.: Environmental security in Arctic ice-covered seas: From strategy to tactics of hazard identification and emergency response, Marine Technology Society Journal, 45, 37–48, 2011.

Eidhammer, T., DeMott, P., Prenni, A., Petters, M., Twohy, C., Rogers, D., Stith, J., Heymsfield, A., Wang, Z., Pratt, K., et al.: Ice initiation by aerosol particles: Measured and predicted ice nuclei concentrations versus measured ice crystal concentrations in an orographic wave
970 cloud, Journal of the Atmospheric Sciences, 67, 2417–2436, 2010.

Emmons, L. K., Walters, S., Hess, P. G., Lamarque, J.-F., Pfister, G. G., Fillmore, D., Granier, C., Guenther, A., Kinnison, D., Laepple, T., et al.: Description and evaluation of the Model for Ozone and Related chemical Tracers, version 4 (MOZART-4), Geoscientific Model Development, 3, 43–67, 2010.

Fan, S.-M. and Jacob, D. J.: Surface ozone depletion in Arctic spring sustained by bromine reactions on aerosols, Nature, 359, 522–524,
975 1992.

Fast, J. D., Gustafson Jr, W. I., Easter, R. C., Zaveri, R. A., Barnard, J. C., Chapman, E. G., Grell, G. A., and Peckham, S. E.: Evolution of ozone, particulates, and aerosol direct radiative forcing in the vicinity of Houston using a fully coupled meteorology-chemistry-aerosol model, Journal of Geophysical Research: Atmospheres, 111, 2006.

Fisher, J. A., Jacob, D. J., Wang, Q., Bahreini, R., Carouge, C. C., Cubison, M. J., Dibb, J. E., Diehl, T., Jimenez, J. L., Leibensperger,
980 E. M., et al.: Sources, distribution, and acidity of sulfate–ammonium aerosol in the Arctic in winter–spring, Atmospheric Environment, 45, 7301–7318, 2011.

Freud, E., Krejci, R., Tunved, P., Leaitch, R., Nguyen, Q. T., Massling, A., Skov, H., and Barrie, L.: Pan-Arctic aerosol number size distributions: seasonality and transport patterns, Atmospheric Chemistry and Physics, 17, 8101–8128, 2017.

Frey, M. M., Norris, S. J., Brooks, I. M., Anderson, P. S., Nishimura, K., Yang, X., Jones, A. E., Nerentorp Mastromonaco, M. G., Jones,
985 D. H., and Wolff, E. W.: First direct observation of sea salt aerosol production from blowing snow above sea ice, Atmospheric Chemistry and Physics, 20, 2549–2578, 2020.

Frossard, A. A., Shaw, P. M., Russell, L. M., Kroll, J. H., Canagaratna, M. R., Worsnop, D. R., Quinn, P. K., and Bates, T. S.: Springtime Arctic haze contributions of submicron organic particles from European and Asian combustion sources, Journal of Geophysical Research: Atmospheres, 116, 2011.

990 Frossard, A. A., Russell, L. M., Burrows, S. M., Elliott, S. M., Bates, T. S., and Quinn, P. K.: Sources and composition of submicron organic mass in marine aerosol particles, Journal of Geophysical Research: Atmospheres, 119, 12,977–13,003, https://doi.org/https://doi.org/10.1002/2014JD021913, 2014.

Fuentes, E., Coe, H., Green, D., Leeuw, G. d., and McFiggans, G.: On the impacts of phytoplankton-derived organic matter on the properties of the primary marine aerosol–Part 1: Source fluxes, Atmospheric Chemistry and Physics, 10, 9295–9317, 2010.

995 Fuentes, E., Coe, H., Green, D., and McFiggans, G.: On the impacts of phytoplankton-derived organic matter on the properties of the primary marine aerosol–Part 2: Composition, hygroscopicity and cloud condensation activity, Atmospheric Chemistry and Physics, 11, 2585–2602, 2011.

Fujiki, T., Matsumoto, K., Honda, M. C., Kawakami, H., and Watanabe, S.: Phytoplankton composition in the subarctic North Pacific during autumn 2005, Journal of plankton research, 31, 179–191, 2009.

1000 Gantt, B., Kelly, J., and Bash, J.: Updating sea spray aerosol emissions in the Community Multiscale Air Quality (CMAQ) model version 5.0. 2, Geoscientific Model Development, 8, 3733–3746, 2015.

Gong, S.: A parameterization of sea-salt aerosol source function for sub-and super-micron particles, Global biogeochemical cycles, 17, 2003.

Gong, S., Barrie, L., and Blanchet, J.-P.: Modeling sea-salt aerosols in the atmosphere: 1. Model development, Journal of Geophysical Research: Atmospheres, 102, 3805–3818, 1997.

1005 Grell, G. A., Dudhia, J., Stauffer, D. R., et al.: A description of the fifth-generation Penn State/NCAR Mesoscale Model (MM5), 1994.

Grell, G. A., Peckham, S. E., Schmitz, R., McKeen, S. A., Frost, G., Skamarock, W. C., and Eder, B.: Fully coupled "online" chemistry within the WRF model, Atmospheric Environment, 39, 6957–6975, 2005.

Grythe, H., Ström, J., Krejci, R., Quinn, P., and Stohl, A.: A review of sea-spray aerosol source functions using a large global set of sea salt aerosol concentration measurements, Atmospheric Chemistry and Physics, 14, 1277–1297, 2014.

1010 Guenther, A., Jiang, X., Heald, C. L., Sakulyanontvittaya, T., Duhl, T., Emmons, L., and Wang, X.: The Model of Emissions of Gases and Aerosols from Nature version 2.1 (MEGAN2. 1): an extended and updated framework for modeling biogenic emissions, Geoscientific Model Development, 5, 1471–1492, 2012.

Hancke, K., Lund-Hansen, L. C., Lamare, M. L., Højlund Pedersen, S., King, M. D., Andersen, P., and Sorrell, B. K.: Extreme low light requirement for algae growth underneath sea ice: A case study from Station Nord, NE Greenland, Journal of Geophysical Research:
1015 Oceans, 123, 985–1000, 2018.

Hara, K., Osada, K., Matsunaga, K., Iwasaka, Y., Shibata, T., and Furuya, K.: Atmospheric inorganic chlorine and bromine species in Arctic boundary layer of the winter/spring, Journal of Geophysical Research: Atmospheres, 107, AAC–4, 2002.

Hartery, S., Toohey, D., Revell, L., Sellegri, K., Kuma, P., Harvey, M., and McDonald, A. J.: Constraining the surface flux of sea spray particles from the Southern Ocean, Journal of Geophysical Research: Atmospheres, 125, e2019JD032 026, 2020.

1020 Heidam, N., Christensen, J., Skov, H., and Wåhlin, P.: Monitoring and modelling of the atmospheric environment in Greenland. A review, Sci Total Environ, 331, 5–28, 2004.

Hirdman, D., Sodemann, H., Eckhardt, S., Burkhart, J. F., Jefferson, A., Mefford, T., Quinn, P. K., Sharma, S., Ström, J., and Stohl, A.: Source identification of short-lived air pollutants in the Arctic using statistical analysis of measurement data and particle dispersion model output, Atmospheric Chemistry and Physics, 10, 669–693, 2010.

1025 Hodnebrog, Ø., Marelle, L., Alterskjær, K., Wood, R. R., Ludwig, R., Fischer, E. M., Richardson, T., Forster, P., Sillmann, J., and Myhre, G.: Intensification of summer precipitation with shorter time-scales in Europe, Environmental Research Letters, 14, 124 050, 2019.

Hong, S.-Y., Noh, Y., and Dudhia, J.: A new vertical diffusion package with an explicit treatment of entrainment processes, Monthly weather review, 134, 2318–2341, 2006.

Horowitz, H. M., Holmes, C., Wright, A., Sherwen, T., Wang, X., Evans, M., Huang, J., Jaeglé, L., Chen, Q., Zhai, S., and Alexan-
1030 der, B.: Effects of Sea Salt Aerosol Emissions for Marine Cloud Brightening on Atmospheric Chemistry: Implications for Radiative

Forcing, Geophysical Research Letters, 47, e2019GL085 838, https://doi.org/https://doi.org/10.1029/2019GL085838, e2019GL085838 2019GL085838, 2020.

Huang, J. and Jaeglé, L.: Wintertime enhancements of sea salt aerosol in polar regions consistent with a sea ice source from blowing snow, Atmospheric Chemistry and Physics, 17, 3699–3712, https://doi.org/10.5194/acp-17-3699-2017, 2017.

1035   Iacono, M. J., D. J. S. M. E. J. S. M. W. C. S. A. and D., C. W.: Radiative forcing by long–lived greenhouse gases: Calculations with the AER radiative transfer models, J. Geophys. Res., 113, https://doi.org/doi: 10.1029/2008JD009944, 2008.

Jacobi, H., Voisin, D., Jaffrezo, J., Cozic, J., and Douglas, T.: Chemical composition of the snowpack during the OASIS spring campaign 2009 at Barrow, Alaska, Journal of Geophysical Research: Atmospheres, 117, 2012.

Jaeglé, L., Quinn, P. K., Bates, T. S., Alexander, B., and Lin, J.-T.: Global distribution of sea salt aerosols: new constraints from in situ and
1040   remote sensing observations, Atmospheric Chemistry and Physics, 11, 3137–3157, https://doi.org/10.5194/acp-11-3137-2011, 2011.

Jiménez, P. A., Dudhia, J., González-Rouco, J. F., Navarro, J., Montávez, J. P., and García-Bustamante, E.: A revised scheme for the WRF surface layer formulation, Monthly weather review, 140, 898–918, 2012.

Jordan, R.: A One-dimensional temperature model for a snow cover : technical documentation for SNTHERM.89, 1991.

Kelly, J. T., Bhave, P. V., Nolte, C. G., Shankar, U., and Foley, K. M.: Simulating emission and chemical evolution of coarse sea-salt particles
1045   in the Community Multiscale Air Quality (CMAQ) model, Geoscientific Model Development, 3, 257–273, https://doi.org/10.5194/gmd-3-257-2010, 2010.

Kirpes, R. M., Bondy, A. L., Bonanno, D., Moffet, R. C., Wang, B., Laskin, A., Ault, A. P., and Pratt, K. A.: Secondary sulfate is internally mixed with sea spray aerosol and organic aerosol in the winter Arctic, Atmospheric Chemistry and Physics, 18, 3937–3949, https://doi.org/10.5194/acp-18-3937-2018, 2018.

1050   Kirpes, R. M., Bonanno, D., May, N. W., Fraund, M., Barget, A. J., Moffet, R. C., Ault, A. P., and Pratt, K. A.: Wintertime Arctic Sea Spray Aerosol Composition Controlled by Sea Ice Lead Microbiology, ACS Central Science, 5, 1760–1767, https://doi.org/10.1021/acscentsci.9b00541, 2019.

Kolesar, K. R., Cellini, J., Peterson, P. K., Jefferson, A., Tuch, T., Birmili, W., Wiedensohler, A., and Pratt, K. A.: Effect of Prudhoe Bay emissions on atmospheric aerosol growth events observed in Utqiaġvik (Barrow), Alaska, Atmospheric Environment, 152, 146–155,
1055   https://doi.org/https://doi.org/10.1016/j.atmosenv.2016.12.019, 2017.

Krembs, C., Eicken, H., Junge, K., and Deming, J.: High concentrations of exopolymeric substances in Arctic winter sea ice: implications for the polar ocean carbon cycle and cryoprotection of diatoms, Deep Sea Research Part I: Oceanographic Research Papers, 49, 2163–2181, https://doi.org/https://doi.org/10.1016/S0967-0637(02)00122-X, 2002.

Lange, R., Dall'Osto, M., Skov, H., Nøjgaard, J., Nielsen, I., Beddows, D., Simó, R., Harrison, R. M., and Massling, A.: Characterization of
1060   distinct Arctic aerosol accumulation modes and their sources, Atmospheric Environment, 183, 1–10, 2018.

Law, K. S., Stohl, A., Quinn, P. K., Brock, C. A., Burkhart, J. F., Paris, J.-D., Ancellet, G., Singh, H. B., Roiger, A., Schlager, H., et al.: Arctic air pollution: New insights from POLARCAT-IPY, Bulletin of the American Meteorological Society, 95, 1873–1895, 2014.

Law, K. S., Roiger, A., Thomas, J. L., Marelle, L., Raut, J.-C., Dalsøren, S., Fuglestvedt, J., Tuccella, P., Weinzierl, B., and Schlager, H.: Local Arctic air pollution: Sources and impacts, Ambio, 46, 453–463, 2017.

1065   Leaitch, W. R., Russell, L. M., Liu, J., Kolonjari, F., Toom, D., Huang, L., Sharma, S., Chivulescu, A., Veber, D., and Zhang, W.: Organic functional groups in the submicron aerosol at 82.5° N, 62.5° W from 2012 to 2014, Atmospheric Chemistry and Physics, 18, 3269–3287, https://doi.org/10.5194/acp-18-3269-2018, 2018.

Leck, C., Norman, M., Bigg, E. K., and Hillamo, R.: Chemical composition and sources of the high Arctic aerosol relevant for cloud forma-
tion, Journal of Geophysical Research: Atmospheres, 107, AAC 1–1–AAC 1–17, https://doi.org/https://doi.org/10.1029/2001JD001463,
2002.

Lee, J., McFiggans, G., Allan, J., Baker, A., Ball, S., Benton, A., Carpenter, L., Commane, R., Finley, B., Evans, M., et al.: Reactive halogens
in the marine boundary layer (RHaMBLe): the tropical North Atlantic experiments, Atmospheric Chemistry and Physics, 10, 1031–1055,
2010.

Li, J., Han, Z., and Yao, X.: A modeling study of the influence of sea salt on inorganic aerosol concentration, size distribution, and deposition
in the western Pacific Ocean, Atmospheric environment, 188, 157–173, 2018.

Liu, J., Gunsch, M. J., Moffett, C. E., Xu, L., El Asmar, R., Zhang, Q., Watson, T. B., Allen, H. M., Crounse, J. D., St. Clair, J., et al.:
Hydroxymethanesulfonate (HMS) formation during summertime fog in an Arctic oil field, Environmental Science & Technology Letters,
8, 511–518, 2021a.

Liu, S., Liu, C.-C., Froyd, K. D., Schill, G. P., Murphy, D. M., Bui, T. P., Dean-Day, J. M., Weinzierl, B., Dollner, M., Diskin, G. S., et al.:
Sea spray aerosol concentration modulated by sea surface temperature, Proceedings of the National Academy of Sciences, 118, 2021b.

Lovejoy, C., Vincent, W. F., Bonilla, S., Roy, S., Martineau, M.-J., Terrado, R., Potvin, M., Massana, R., and Pedrós-Alió, C.: DISTRIBU-
TION, PHYLOGENY, AND GROWTH OF COLD-ADAPTED PICOPRASINOPHYTES IN ARCTIC SEAS 1, Journal of Phycology,
43, 78–89, 2007.

Lovejoy C., W. F. Vincent, S. B. S. R. M.-J. M. R. T. M. P. R. M. C. P.: Distribution, Phylogeny, and Growth of Cold-Adapted Picoprasino-
phytes in Arctic Seas, J. Phycol., 43, 78–89, https://doi.org/https://doi.org/10.1111/j.1529-8817.2006.00310.x, 2007.

Ma, X., von Salzen, K., and Li, J.: Modelling sea salt aerosol and its direct and indirect effects on climate, Atmospheric Chemistry and
Physics, 8, 1311–1327, https://doi.org/10.5194/acp-8-1311-2008, 2008.

Malm, W. C., Sisler, J. F., Huffman, D., Eldred, R. A., and Cahill, T. A.: Spatial and seasonal trends in particle con-
centration and optical extinction in the United States, Journal of Geophysical Research: Atmospheres, 99, 1347–1370,
https://doi.org/https://doi.org/10.1029/93JD02916, 1994.

Marelle, L., Raut, J.-C., Law, K. S., Berg, L. K., Fast, J. D., Easter, R. C., Shrivastava, M., and Thomas, J. L.: Improvements to the WRF-Chem
3.5.1 model for quasi-hemispheric simulations of aerosols and ozone in the Arctic, Geoscientific Model Development, 10, 3661–3677,
https://doi.org/10.5194/gmd-10-3661-2017, 2017.

Marelle, L., Thomas, J. L., Ahmed, S., Tuite, K., Stutz, J., Dommergue, A., Simpson, W. R., Frey, M. M., and Baladima, F.: Implementation
and Impacts of Surface and Blowing Snow Sources of Arctic Bromine Activation Within WRF-Chem 4.1.1, Journal of Advances in Mod-
eling Earth Systems, 13, e2020MS002 391, https://doi.org/https://doi.org/10.1029/2020MS002391, e2020MS002391 2020MS002391,
2021.

May, N. W., Quinn, P. K., McNamara, S. M., and Pratt, K. A.: Multiyear study of the dependence of sea salt aerosol on
wind speed and sea ice conditions in the coastal Arctic, Journal of Geophysical Research: Atmospheres, 121, 9208–9219,
https://doi.org/https://doi.org/10.1002/2016JD025273, 2016.

Millero, F. J., Feistel, R., Wright, D. G., and McDougall, T. J.: The composition of Standard Seawater and the defini-
tion of the Reference-Composition Salinity Scale, Deep Sea Research Part I: Oceanographic Research Papers, 55, 50–72,
https://doi.org/https://doi.org/10.1016/j.dsr.2007.10.001, 2008.

Monaghan, A. J., Clark, M. P., Barlage, M. P., Newman, A. J., Xue, L., Arnold, J. R., and Rasmussen, R. M.: High-Resolution Historical Climate Simulations over Alaska, Journal of Applied Meteorology and Climatology, 57, 709–731, https://www.jstor.org/stable/26501015, 2018.

Monahan, E. and Muircheartaigh, I.: Optimal Power-Law Description of Oceanic Whitecap Coverage Dependence on Wind Speed, Journal of Physical Oceanography, 10, 2094–2099, 1980.

Monahan, E., Spiel, D. E., and Davidson, K.: A Model of Marine Aerosol Generation Via Whitecaps and Wave Disruption, 1986.

Morrison, H., T. G. T. V.: Impact of Cloud Microphysics on the Development of Trailing Stratiform Precipitation in a Simulated Squall Line: Comparison of One– and Two–Moment Schemes, Mon. Wea. Rev., 137, 991—-1007, https://doi.org/10.1175/2008MWR2556.1, 2009.

Moschos, V., Dzepina, K., Bhattu, D., Lamkaddam, H., Casotto, R., Daellenbach, K. R., Canonaco, F., Rai, P., Aas, W., Becagli, S., et al.: Equal abundance of summertime natural and wintertime anthropogenic Arctic organic aerosols, Nature geoscience, 15, 196–202, 2022a.

Moschos, V., Schmale, J., Aas, W., Becagli, S., Calzolai, G., Eleftheriadis, K., Moffett, C. E., Schnelle-Kreis, J., Severi, M., Sharma, S., et al.: Elucidating the present-day chemical composition, seasonality and source regions of climate-relevant aerosols across the Arctic land surface, Environmental Research Letters, 17, 034 032, 2022b.

NCEP: National Centers for Environmental Prediction, National Weather Service, NOAA, U.S. Department of Commerce, NCEP FNL Operational Model Global Tropospheric Analyses, continuing from July 1999, https://doi.org/10.5065/D6M043C6, 2000.

Neumann, D., Matthias, V., Bieser, J., Aulinger, A., and Quante, M.: Sensitivity of modeled atmospheric nitrogen species and nitrogen deposition to variations in sea salt emissions in the North Sea
and Baltic Sea regions, Atmospheric Chemistry and Physics, 16, 2921–2942, https://doi.org/10.5194/acp-16-2921-2016, 2016.

Nielsen, I. E., Skov, H., Massling, A., Eriksson, A. C., Dall'Osto, M., Junninen, H., Sarnela, N., Lange, R., Collier, S., Zhang, Q., et al.: Biogenic and anthropogenic sources of aerosols at the High Arctic site Villum Research Station, Atmospheric Chemistry and Physics, 19, 10 239–10 256, 2019.

Niu, G.-Y. and Yang, Z.-L.: Effects of vegetation canopy processes on snow surface energy and mass balances, Journal of Geophysical Research: Atmospheres, 109, https://doi.org/https://doi.org/10.1029/2004JD004884, 2004.

Niu, G.-Y. and Yang, Z.-L.: Effects of frozen soil on snowmelt runoff and soil water storage at a continental scale, Journal of Hydrometeorology, 7, 937–952, 2006.

Niu, G.-Y., Yang, Z.-L., Dickinson, R. E., Gulden, L. E., and Su, H.: Development of a simple groundwater model for use in climate models and evaluation with Gravity Recovery and Climate Experiment data, Journal of Geophysical Research: Atmospheres, 112, https://doi.org/https://doi.org/10.1029/2006JD007522, 2007.

Niu, G.-Y., Yang, Z.-L., Mitchell, K. E., Chen, F., Ek, M. B., Barlage, M., Kumar, A., Manning, K., Niyogi, D., Rosero, E., Tewari, M., and Xia, Y.: The community Noah land surface model with multiparameterization options (Noah-MP): 1. Model description and evaluation with local-scale measurements, Journal of Geophysical Research: Atmospheres, 116, https://doi.org/https://doi.org/10.1029/2010JD015139, 2011.

O'Dowd, C. D., Smith, M. H., Consterdine, I. E., and Lowe, J. A.: Marine aerosol, sea-salt, and the marine sulphur cycle: a short review, Atmospheric Environment, 31, 73–80, https://doi.org/https://doi.org/10.1016/S1352-2310(96)00106-9, 1997.

O'Dowd, C. D., Facchini, M. C., Cavalli, F., Ceburnis, D., Mircea, M., Decesari, S., Fuzzi, S., Yoon, Y. J., and Putaud, J.-P.: Biogenically driven organic contribution to marine aerosol, Nature, 431, 676–680, 2004.

Ovadnevaite, J., Ceburnis, D., Martucci, G., Bialek, J., Monahan, C., Rinaldi, M., Facchini, M. C., Berresheim, H., Worsnop, D. R., and O'Dowd, C.: Primary marine organic aerosol: A dichotomy of low hygroscopicity and high CCN activity, Geophysical Research Letters, 38, https://doi.org/https://doi.org/10.1029/2011GL048869, 2011.

Ovadnevaite, J., Ceburnis, D., Canagaratna, M., Berresheim, H., Bialek, J., Martucci, G., Worsnop, D. R., and O'Dowd, C.: On the effect of wind speed on submicron sea salt mass concentrations and source fluxes, Journal of Geophysical Research: Atmospheres, 117, 2012.

Ovadnevaite, J., Manders, A., de Leeuw, G., Ceburnis, D., Monahan, C., Partanen, A.-I., Korhonen, H., and O'Dowd, C. D.: A sea spray aerosol flux parameterization encapsulating wave state, Atmospheric Chemistry and Physics, 14, 1837–1852, https://doi.org/10.5194/acp-14-1837-2014, 2014.

Partanen, A.-I., Dunne, E., Bergman, T., Laakso, A., Kokkola, H., Ovadnevaite, J., Sogacheva, L., Baisnée, D., Sciare, J., Manders, A., et al.: Global modelling of direct and indirect effects of sea spray aerosol using a source function encapsulating wave state, Atmospheric Chemistry and Physics, 14, 11 731–11 752, 2014.

Peterson, P. K., Pöhler, D., Sihler, H., Zielcke, J., General, S., Frieß, U., Platt, U., Simpson, W. R., Nghiem, S. V., Shepson, P. B., et al.: Observations of bromine monoxide transport in the Arctic sustained on aerosol particles, Atmospheric Chemistry and Physics, 17, 7567–7579, 2017.

Quinn, P., Coffman, D., Johnson, J., Upchurch, L., and Bates, T.: Small fraction of marine cloud condensation nuclei made up of sea spray aerosol, Nature Geoscience, 10, 674–679, 2017.

Quinn, P. K., Coffman, D. J., Kapustin, V. N., Bates, T. S., and Covert, D. S.: Aerosol optical properties in the marine boundary layer during the First Aerosol Characterization Experiment (ACE 1) and the underlying chemical and physical aerosol properties, Journal of Geophysical Research: Atmospheres, 103, 16 547–16 563, https://doi.org/https://doi.org/10.1029/97JD02345, 1998.

Quinn, P. K., Miller, T. L., Bates, T. S., Ogren, J. A., Andrews, E., and Shaw, G. E.: A 3-year record of simultaneously measured aerosol chemical and optical properties at Barrow, Alaska, Journal of Geophysical Research: Atmospheres, 107, AAC 8–1–AAC 8–15, https://doi.org/https://doi.org/10.1029/2001JD001248, 2002.

Quinn, P. K., SHAW, G., ANDREWS, E., DUTTON, E. G., RUOHO-AIROLA, T., and GONG, S. L.: Arctic haze: current trends and knowledge gaps, Tellus B, 59, 99–114, https://doi.org/https://doi.org/10.1111/j.1600-0889.2006.00238.x, 2007.

Rahn, K. A. and McCaffrey, R. J.: On the origin and transport of the winter Arctic aerosol, Annals of the New York Academy of Sciences, 338, 486–503, 1980.

Raut, J.-C., Marelle, L., Fast, J. D., Thomas, J. L., Weinzierl, B., Law, K. S., Berg, L. K., Roiger, A., Easter, R. C., Heimerl, K., et al.: Cross-polar transport and scavenging of Siberian aerosols containing black carbon during the 2012 ACCESS summer campaign, Atmospheric Chemistry and Physics, 17, 10 969–10 995, 2017.

Revell, L. E., Kremser, S., Hartery, S., Harvey, M., Mulcahy, J. P., Williams, J., Morgenstern, O., McDonald, A. J., Varma, V., Bird, L., and Schuddeboom, A.: The sensitivity of Southern Ocean aerosols and cloud microphysics to sea spray and sulfate aerosol production in the HadGEM3-GA7.1 chemistry–climate model, Atmospheric Chemistry and Physics, 19, 15 447–15 466, https://doi.org/10.5194/acp-19-15447-2019, 2019.

Rhodes, R. H., Yang, X., Wolff, E. W., McConnell, J. R., and Frey, M. M.: Sea ice as a source of sea salt aerosol to Greenland ice cores: a model-based study, Atmospheric Chemistry and Physics, 17, 9417–9433, https://doi.org/10.5194/acp-17-9417-2017, 2017.

Roscoe, H. K., Brooks, B., Jackson, A., Smith, M., Walker, S., Obbard, R. W., and Wolff, E. W.: Frost flowers in the laboratory: Growth, characteristics, aerosol, and the underlying sea ice, Journal of Geophysical Research: Atmospheres, 116, 2011.

Russell, L. M., Hawkins, L. N., Frossard, A. A., Quinn, P. K., and Bates, T. S.: Carbohydrate-like composition of submicron atmospheric particles and their production from ocean bubble bursting, Proceedings of the National Academy of Sciences, 107, 6652–6657, https://doi.org/10.1073/pnas.0908905107, 2010.

Sakaguchi, K. and Zeng, X.: Effects of soil wetness, plant litter, and under-canopy atmospheric stability on ground evaporation in the Community Land Model (CLM3.5), Journal of Geophysical Research: Atmospheres, 114, https://doi.org/https://doi.org/10.1029/2008JD010834, 2009.

Saliba, G., Chen, C.-L., Lewis, S., Russell, L. M., Rivellini, L.-H., Lee, A. K. Y., Quinn, P. K., Bates, T. S., Haëntjens, N., Boss, E. S., Karp-Boss, L., Baetge, N., Carlson, C. A., and Behrenfeld, M. J.: Factors driving the seasonal and hourly variability of sea-spray aerosol number in the North Atlantic, Proceedings of the National Academy of Sciences, 116, 20 309–20 314, https://doi.org/10.1073/pnas.1907574116, 2019.

Salisbury, D. J., Anguelova, M. D., and Brooks, I. M.: On the variability of whitecap fraction using satellite-based observations, Journal of Geophysical Research: Oceans, 118, 6201–6222, 2013.

Salisbury, D. J., Anguelova, M. D., and Brooks, I. M.: Global distribution and seasonal dependence of satellite-based whitecap fraction, Geophysical Research Letters, 41, 1616–1623, https://doi.org/https://doi.org/10.1002/2014GL059246, 2014.

Salter, M. E., Zieger, P., Acosta Navarro, J. C., Grythe, H., Kirkevåg, A., Rosati, B., Riipinen, I., and Nilsson, E. D.: An empirically derived inorganic sea spray source function incorporating sea surface temperature, Atmospheric Chemistry and Physics, 15, 11 047–11 066, https://doi.org/10.5194/acp-15-11047-2015, 2015.

Schmale, J., Arnold, S., Law, K. S., Thorp, T., Anenberg, S., Simpson, W., Mao, J., and Pratt, K.: Local Arctic air pollution: A neglected but serious problem, Earth's Future, 6, 1385–1412, 2018.

Schmale, J., Sharma, S., Decesari, S., Pernov, J., Massling, A., Hansson, H.-C., Von Salzen, K., Skov, H., Andrews, E., Quinn, P. K., et al.: Pan-Arctic seasonal cycles and long-term trends of aerosol properties from 10 observatories, Atmospheric Chemistry and Physics, 22, 3067–3096, 2022.

Seinfeld, J. and Pandis, S.: Atmospheric Chemistry and Physics: From Air Pollution to Climate Change, 1998.

Sellers, P., Randall, D., Collatz, G., Berry, J., Field, C., Dazlich, D., Zhang, C., Collelo, G., and Bounoua, L.: A revised Land Surface parameterization (SiB2) for atmospheric GCMs. Part I: Model Formulation, Journal of Climate, 9, 676–705, https://doi.org/10.1175/1520-0442(1996)009<0676:ARLSPF>2.0.CO;2, 1996.

Sharma, S., Barrie, L. A., Magnusson, E., Brattström, G., Leaitch, W., Steffen, A., and Landsberger, S.: A factor and trends analysis of multidecadal lower tropospheric observations of Arctic aerosol composition, black carbon, ozone, and mercury at Alert, Canada, Journal of Geophysical Research: Atmospheres, 124, 14 133–14 161, 2019.

Shaw, P. M., Russell, L. M., Jefferson, A., and Quinn, P. K.: Arctic organic aerosol measurements show particles from mixed combustion in spring haze and from frost flowers in winter, Geophysical Research Letters, 37, https://doi.org/https://doi.org/10.1029/2010GL042831, 2010.

Shaw, W. J., Jerry Allwine, K., Fritz, B. G., Rutz, F. C., Rishel, J. P., and Chapman, E. G.: An evaluation of the wind erosion module in DUSTRAN, Atmospheric Environment, 42, 1907–1921, https://doi.org/https://doi.org/10.1016/j.atmosenv.2007.11.022, 2008.

Sheridan, P., Delene, D., and Ogren, J.: Four years of continuous surface aerosol measurements from the Department of Energy's Atmospheric Radiation measurement Program Southern Great Plains Cloud and Radiation Testbed site, Journal of Geophysical Research: Atmospheres, 106, 20 735–20 747, 2001.

Shrivastava, M., Fast, J., Easter, R., Gustafson Jr., W. I., Zaveri, R. A., Jimenez, J. L., Saide, P., and Hodzic, A.: Modeling organic aerosols in a megacity: comparison of simple and complex representations of the volatility basis set approach, Atmospheric Chemistry and Physics, 11, 6639–6662, https://doi.org/10.5194/acp-11-6639-2011, 2011.

Simpson, W., Carlson, D., Hönninger, G., Douglas, T., Sturm, M., Perovich, D., and Platt, U.: First-year sea-ice contact predicts bromine monoxide (BrO) levels at Barrow, Alaska better than potential frost flower contact, Atmospheric Chemistry and Physics, 7, 621–627, 2007.

Sofiev, M., Soares, J., Prank, M., de Leeuw, G., and Kukkonen, J.: A regional-to-global model of emission and transport of sea salt particles in the atmosphere, Journal of Geophysical Research: Atmospheres, 116, https://doi.org/https://doi.org/10.1029/2010JD014713, 2011.

Spada, M., Jorba, O., Pérez García-Pando, C., Janjic, Z., and Baldasano, J. M.: Modeling and evaluation of the global sea-salt aerosol distribution: sensitivity to size-resolved and sea-surface temperature dependent emission schemes, Atmospheric Chemistry and Physics, 13, 11 735–11 755, https://doi.org/10.5194/acp-13-11735-2013, 2013.

Stroeve, J., Serreze, M., Holland, M., Kay, J., Malanik, J., and Barrett, A.: The Arctic's rapidly shrinking sea ice cover: a research synthesis, Climatic Change, 110, 1005–1027, https://doi.org/10.1007/s10584-011-0101-1, 2012.

Su, B., Wang, T., Zhang, G., Liang, Y., Lv, C., Hu, Y., Li, L., Zhou, Z., Wang, X., and Bi, X.: A review of atmospheric aging of sea spray aerosols: Potential factors affecting chloride depletion, Atmospheric Environment, p. 119365, 2022.

Wang, X., Jacob, D. J., Eastham, S. D., Sulprizio, M. P., Zhu, L., Chen, Q., Alexander, B., Sherwen, T., Evans, M. J., Lee, B. H., et al.: The role of chlorine in global tropospheric chemistry, Atmospheric Chemistry and Physics, 19, 3981–4003, 2019.

Whaley, C. H., Mahmood, R., von Salzen, K., Winter, B., Eckhardt, S., Arnold, S., Beagley, S., Becagli, S., Chien, R.-Y., Christensen, J., Damani, S. M., Eleftheriadis, K., Evangeliou, N., Faluvegi, G. S., Flanner, M., Fu, J. S., Gauss, M., Giardi, F., Gong, W., Hjorth, J. L., Huang, L., Im, U., Kanaya, Y., Krishnan, S., Klimont, Z., Kühn, T., Langner, J., Law, K. S., Marelle, L., Massling, A., Olivié, D., Onishi, T., Oshima, N., Peng, Y., Plummer, D. A., Popovicheva, O., Pozzoli, L., Raut, J.-C., Sand, M., Saunders, L. N., Schmale, J., Sharma, S., Skov, H., Taketani, F., Thomas, M. A., Traversi, R., Tsigaridis, K., Tsyro, S., Turnock, S., Vitale, V., Walker, K. A., Wang, M., Watson-Parris, D., and Weiss-Gibbons, T.: Model evaluation of short-lived climate forcers for the Arctic Monitoring and Assessment Programme: a multi-species, multi-model study, Atmospheric Chemistry and Physics Discussions, 2022, 1–88, https://doi.org/10.5194/acp-2021-975, 2022.

Wild, O., Zhu, X., and Prather, M.: Fast-J: Accurate Simulation of In- and Below-Cloud Photolysis in Tropospheric Chemical Models, Journal of Atmospheric Chemistry, 37, 245–282, 2000.

Wu, S.-P., Dai, L.-H., Zhu, H., Zhang, N., Yan, J.-P., Schwab, J. J., and Yuan, C.-S.: The impact of sea-salt aerosols on particulate inorganic nitrogen deposition in the western Taiwan Strait region, China, Atmospheric Research, 228, 68–76, 2019.

Xu, L., Russell, L. M., Somerville, R. C. J., and Quinn, P. K.: Frost flower aerosol effects on Arctic wintertime longwave cloud radiative forcing, Journal of Geophysical Research: Atmospheres, 118, 13,282–13,291, https://doi.org/https://doi.org/10.1002/2013JD020554, 2013.

Xu, L., Russell, L. M., and Burrows, S. M.: Potential sea salt aerosol sources from frost flowers in the pan-Arctic region, Journal of Geophysical Research: Atmospheres, 121, 10,840–10,856, https://doi.org/https://doi.org/10.1002/2015JD024713, 2016.

Xu, W., Ovadnevaite, J., Fossum, K. N., Lin, C., Huang, R.-J., Ceburnis, D., and O'Dowd, C.: Sea spray as an obscured source for marine cloud nuclei, Nature Geoscience, 15, 282–286, 2022.

Yang, R. and Friedl, M. A.: Modeling the effects of three-dimensional vegetation structure on surface radiation and energy balance in boreal forests, Journal of Geophysical Research: Atmospheres, 108, https://doi.org/https://doi.org/10.1029/2002JD003109, 2003.

Yang Z.-L., R. E. Dickinson, A. R. and Vinnikov., K. Y.: Validation of the snow sub-model of the Biosphere-Atmosphere Transfer Scheme with Russian snow cover and meteorological observational data, J. Clim., 10, 353—-373, https://doi.org/10.1175/1520-0442(1997)010<0353:VOTSSO>2.0.CO;2, 1997.

1255   yue Niu, G. and liang Yang, Z.: Effects of frozen soil on snowmelt runoff and soil water storage at a continental scale, J. Hydrometeorol, pp. 937–952, 2006.

Zaveri, R. A., Easter, R. C., Fast, J. D., and Peters, L. K.: Model for Simulating Aerosol Interactions and Chemistry (MOSAIC), Journal of Geophysical Research: Atmospheres, 113, https://doi.org/https://doi.org/10.1029/2007JD008782, 2008.

Zhao, C. and Garrett, T. J.: Effects of Arctic haze on surface cloud radiative forcing, Geophysical Research Letters, 42, 557–564, 2015.

1260   Zwaaftink, C. G., Grythe, H., Skov, H., and Stohl, A.: Substantial contribution of northern high-latitude sources to mineral dust in the Arctic, Journal of Geophysical Research: Atmospheres, 121, 13–678, 2016.